Extended range simulations of the extreme snow storms over southern China in early 2008 with the BCC_AGCM2.1 model

Anning Huang,[1] Yaocun Zhang,[1] Zaizhi Wang,[2] Tongwun Wu,[2] Danqing Huang,[1] Yang Zhou,[1] Yong Zhao,[3] Ying Huang,[1] Xueyuan Kuang,[1] Lujun Zhang,[1] Yongjie Fang,[2] and Yan Guo[4]

Received 13 January 2013; revised 5 July 2013; accepted 8 July 2013; published 5 August 2013.

[1] The 10–30 day extended range potential predictability of the Beijing Climate Center Atmospheric General Circulation Model version 2.1 (BCC_AGCM2.1) model with high horizontal resolution has been evaluated, and the associated influencing factors and possible physical mechanisms have been discussed through a case study of the long-lasting extreme snow storms over southern China in early 2008. Comparison with meteorological observations suggests that the BCC_AGCM2.1 model forced by the real daily sea surface temperature (SST) well reproduced the extraordinarily frequent and long-lasting heavy snow storm process over southern China in early 2008 including the spatial distribution and temporal evolution of the 2 m air temperature and snow rainfall but produced relatively larger errors in precipitation. Overall, the BCC-AGCM2.1 model forced by the real daily SST shows good potential predictability on 10–30 day extended range time scale to some extent, at least from this extreme snow storm case study. Further analysis of the associated influencing factors and possible physical mechanisms indicates that the SST forcing is not as important as the initial conditions for the weather forecast within around 2 weeks in advance which is the upper limit of the daily weather forecast. However, the SST forcing with relatively larger day-to-day variability plays an important role in the potential predictability of the BCC_AGCM2.1 model on 10–30 day extended forecasting time scale through affecting the atmospheric variability. Results from this study provide us some necessary and valuable information for further development of an operational 10–30 day extended range forecasting system.

Citation: Huang, A., et al. (2013), Extended range simulations of the extreme snow storms over southern China in early 2008 with the BCC_AGCM2.1 model, *J. Geophys. Res. Atmos.*, *118*, 8253–8273, doi:10.1002/jgrd.50638.

1. Introduction

[2] Weather forecasts are expected to offer future meteorological information for a specified region and over a specified period of time. According to the time covered, weather forecasts are classified as short- (< 3 days), medium- (3–10 days), and long- (>10 days) range forecasts. Current short-range forecasts basically are reliable. However, 3–10 day forecasts are less reliable. Useful skill in weather forecasts from present-day numerical weather models typically extends out to about 10 days, and the weather forecasts decline in accuracy with time [*Simmons and Hollingsworth*, 2002]. Present meteorological operations in China only cover the conventional weather forecasts (short- and medium-range weather forecasts) and climate predictions for the periods longer than 1 month. For the lack of objective methods and tools, the forecasts of weather processes for the period over 10–30 days in advance have become a linkage to bridge the time gap between the weather forecast and climate prediction and are described as 10–30 day extended range forecasts, which have been recognized as a basic step for creating an early warning system of severe weather events in China [*Jin et al.*, 2010].

[3] Because of the chaotic characteristics inherent in the atmosphere [*Lorenz*, 1963], the 10–30 day extended range forecasts are beyond the range of predictability of daily weather, but some predictable components, like some planetary scale motions which could be forecasted very well [*Chou et al.*, 2010]. Actually, the time scale of the process itself strongly affects the leading time through which useful forecasts can be obtained [e.g., *Van den Dool and Saha*, 1990]. For example, the evolution of the coupled ocean-atmosphere El Nino-Southern Oscillation phenomena is predictable with lead times of at least 6–9 months [*Cane*

[1]School of Atmospheric Sciences, Nanjing University, Nanjing, China.
[2]Beijing Climate Center, National Climate Center, China Meteorological Administration, Beijing, China.
[3]Institute of Desert Meteorology, China Meteorology Administration, Urumqi, China.
[4]Bao Shan Meteorological Bureau, Baoshan, China.

Corresponding author: A. Huang, School of Atmospheric Sciences, Nanjing University, No. 22 Hankou Rd., Nanjing, Jiangsu 210093, China. (anhuang@nju.edu.cn)

2169-897X/13/10.1002/jgrd.50638

et al., 1986]. In addition, some external forcings, such as soil moisture, snow cover, sea surface temperature (SST), and sea ice, have longer persistence than synoptic scale and can affect the predictability of weather processes [*Smith et al*., 2012]. The 10–30 day extended range forecasts just cover the upper limit of predictability of daily weather and lower time limit of the external forcings and are issues between the weather forecasts and climate predictions. Earlier studies showed that some atmospheric phenomena with long life cycle, such as Madden-Julian oscillation [*Ferranti et al*., 1990; *Chen and Alpert*, 1990], planetary Rossby waves [*Dickinson*, 1968; *Matsuno*, 1970], and Arctic oscillation [*Baldwin et al*., 2003; *Li and Wang*, 2003], have significant impacts on the synoptic scale systems. The predictability of the quasi-steady systems can still be maintained when the individual synoptic systems lose their predictability. The persistence of some anomalous large-scale atmospheric circulations is very helpful to forecast the statistical distribution of weather processes on extended range time scale [*Shukla*, 1981; *Waliser et al*., 1999]. Therefore, being able to predict aspects of low-frequency processes in a numerical model can be extremely valuable to extended range weather and/or short-term climate forecasting. The extended range forecasts do not yet meet the necessary standards for quality and are still in the developmental phase. The compilation of sufficiently accurate extended range forecasts is one of the hardest problems in modern science.

[4] The 10–30 day extended range forecasts play an important role in helping the development of weather business and service for the economic development [*Jin et al*., 2010]. During the past years, a wealth of studies on the 10–30 day extended range forecasts using numerical models have been carried out. *Miyakoda et al*. [1983, 1986] tried to forecast the weather at the time scale of extended range by using a numerical model and aroused the interest in the operational forecasts at time scale of extended range in many weather forecast centers in the world. *Palmer* [1993] discussed the Lorenz model's performance in the extended range prediction and found that the predictability was increased by introducing a memory of the recent past history of the state vector as a forcing in the dynamical equations. *Baumhefner* [1996] evaluated the potential forecast skill of winter 10–30 day extended range predication using a low resolution climate model and found that this model could be a valuable tool for numerical extended range forecasting.

[5] Extraordinarily frequent and long-lasting heavy snow storms in early 2008 [*Gao*, 2009; *Wen et al*., 2009; *Zhou et al*., 2009] affected China and experienced four major periods: 10–16, 18–22, and 25–29 January, and from 31 January to 2 February 2008, resulting in excessive snow amount, low temperatures, and severe icing conditions over southern China. The heavy snow storms show significant 10–20 day and 30–60 day oscillations [*Ma et al*., 2011], and the duration of this episode lasted around 25 days which is in the range of forecast period of the 10–30 day extended range forecasts. This heavy snow storm event over southern China in early 2008 provides a good case to evaluate the 10–30 day extended range potential predictability of Beijing Climate Center Atmospheric General Circulation Model version 2.1 (BCC_AGCM2.1) with high horizontal resolution. Early studies show that the ocean state is crucial for seasonal to decadal predictions. Although observations of sea ice, snow cover, and soil moisture are also potentially important, predictions beyond a couple of weeks rely mainly on the relatively slow time scales in the ocean such as SST [*Rodwell et al*., 1999; *Scaife and Knigh*, 2008; *Smith et al*., 2012]. However, how the SST forcing affects the potential predictability of 10–30 day extended range forecasts, which cover the upper time limit of daily weather forecast and lower time limit of climate prediction, is still unclear so far. The aim of this study is to answer such questions as follows: How is the potential predictability of the BCC_AGCM2.1 model forced by the real daily SST on the 10–30 day extended range forecasting time scale? What are the possible mechanisms for the impact of subseasonal variability of SST forcing on the 10–30 day extended range forecasting?

[6] In section 2, the data and methodology are introduced. The BCC_AGCM2.1 model and experimental design are described in section 3. The analysis of the model results and possible reasons are presented in section 4. A summary of conclusions is provided in section 5.

2. Data and Methodology

2.1. Data

[7] The following data are used for this work: (a) the National Centers for Environmental Prediction/National Center for Atmospheric Research (NCEP/NCAR) reanalysis [*Kalnay et al*., 1996] four times daily data in 1982–2008 with a horizontal resolution of 2.5° latitude by 2.5° longitude, including air temperature, specific humidity, wind components, and geopotential height fields; (b) the National Oceanic and Atmospheric Administration (NOAA) high-resolution daily SST and sea ice concentration data [*Reynolds et al*., 2007] with a horizontal resolution of 0.25° latitude by 0.25° longitude in 1982–2008, which can be obtained from the web site at http://www.esrl.noaa.gov/psd/data/gridded/tables/ocean.html or the ftp address at ftp.cdc.noaa.gov/pub/Datasets/noaa.oisst.v2.highres; and (c) the observed daily precipitation and 2 m air temperature data during 1950–2009 from 756 meteorological stations compiled by the Chinese Meteorological Administration.

2.2. Methodology

[8] The analysis methods including the spatial correlation coefficient (SCC), root-mean-square error (RMSE), standard deviation (SD), and linear regression are adopted in this study. The detailed descriptions for them are given as follows:

[9] 1. Spatial correlation coefficient

[10] The SCC is expressed as

$$\mathrm{SCC} = \frac{\sum_{I=1}^{N}\left(R_{FI}-\overline{R}_F\right)\left(R_{OI}-\overline{R}_O\right)}{\sqrt{\sum_{I=1}^{N}\left(R_{FI}-\overline{R}_F\right)^2\sum_{I=1}^{N}\left(R_{OI}-\overline{R}_O\right)^2}} \tag{1}$$

where N denotes the grid number in an investigated domain. R_{FI} (R_{OI}) are the simulation (observation) of variable R at the Ith grid. $\overline{R}_F = \frac{1}{N}\sum_{I=1}^{N} R_{FI}$ and $\overline{R}_O = \frac{1}{N}\sum_{I=1}^{N} R_{OI}$ are the regionally averaged simulation and observation over the investigated domain, respectively. The SCC can reveal the spatial distribution similarity between the model simulation and the observation [*Huang et al*., 2009]; high SCC indicates that the

Table 1. Experimental Design

Experiment	Initial Condition	SST
RSST	four times daily NCEP/NCAR data on 1–2 January 2008	NOAA daily SST during 1 January to 1 March 2008
SSTA	four times daily NCEP/NCAR data on 1–2 January 2008	NOAA daily climatology of SST during 1 January to 1 March of 1982–2008 plus SST anomalies on 1 January 2008
MEAN	four times daily NCEP/NCAR data on 1 January during 1982–2007	NOAA daily SST during 1 January to 1 March in each year of 1982–2007

simulation shows good similarity with the spatial distribution of the observation.

[11] 2. Root-mean-square error

[12] The RMSE is given by

$$\mathrm{RMSE} = \left\{ \frac{1}{N} \sum_{i=1}^{N} \left(E_i - \overline{E}\right)^2 \right\}^{1/2} \tag{2}$$

where $E_i = E_{fi} - E_{Oi}$ is the difference between the model simulation and the observation, $\overline{E} = \frac{1}{N} \sum_{i=1}^{N} E_i$, and N is the total grid number. Low RMSE indicates that the intensity of the simulation is close to the observation. On the contrary, high RMSE reflects large differences in intensity between the simulation and the observation.

[13] 3. Standard deviation

[14] The SD is given by

$$\mathrm{SD} = \sqrt{\frac{1}{N} \sum_{i=1}^{N} \left(X_i - \overline{X}\right)^2} \tag{3}$$

where $(X_1, X_2, \ldots X_N)$ are the values of the sample items and $\overline{X}$ is their mean value. The denominator N stands for the size of the sample. Low SD indicates that the data points tend to be very close to the mean; however, high SD indicates that the data points are spread out over a large range of values.

[15] 4. Linear regression

[16] The linear regression method [*Kenney and Keeping*, 1962] is used to find the equation of the straight line of n data points $\{y_i, x_i\}$, where $i = 1, 2, \ldots, n$. The linear regression equation is described as

$$\hat{y} = a + bx_i \tag{4}$$

where a is the intercept and b is the slope (also called the regression coefficient), which would provide a "best" fit for the data points. Here the best will be understood as in the least squares approach: such a line that minimizes the sum of squared residuals of the linear regression model. In other words, numbers a and b solve the following minimization problem: find the min $\left(Q(a,b) = \sum_{i=1}^{n} (y_i - \hat{y}_i)^2 \right)$. Based on the least squares approach, the a and b can be calculated as follows:

$$b = \frac{\sum_{i=1}^{n} (x_i - \overline{x})(x_i - \overline{x})}{\sum_{i=1}^{n} (x_i - \overline{x})} = \frac{s_{xy}}{s_x^2} = r_{xy} \frac{s_y}{s_x} \tag{5}$$

$$a = \overline{y} - \beta \overline{x} \tag{6}$$

where s_{xy} is the covariance of x and y variables. s_x (s_y) is the standard deviation of variable x (y). r_{xy} is the correlation coefficient of x and y variables. Horizontal bar over a variable means the sample average of that variable. The linear regression t test given by $t = \sqrt{n-2} \frac{r_{xy}}{\sqrt{1-r_{xy}^2}}$ is used to determine whether the slope of the linear regression is significant, where the degrees of freedom $(n-2)$ can be derived from the sample size n. For simplicity, the correlation coefficient r_c at a given significance level (i.e., 0.05) with $n-2$ degrees of freedom can be derived by $r_c = \sqrt{\frac{t_{\alpha=0.05}^2}{(n-2)+t_{\alpha=0.05}^2}}$. For a given n, we can get a r_c and then the regression over 95% significant confidence level can be determined by $|r_{xy}| \geq r_c$.

3. Model Description and Numerical Experiment Design

3.1. Model Description

[17] The climate model used in this study is Beijing Climate Center Atmospheric General Circulation Model version 2.1 (BCC_AGCM2.1), which is also the atmospheric component in Beijing Climate Center Climate System Model (BCC_CSM1.1) [*Wu et al*., 2013]. The dynamical core of BCC_AGCM2.1 is described by *Wu et al*. [2008]. The model equations originated from the Eulerian dynamic framework of the Community Atmosphere Model version 3 (CAM3) [*Collins et al*., 2006] are formulated in a horizontal T106 spectral resolution (approximately 1° latitude by 1° longitude) and a terrain-following hybrid vertical coordinate with 26 levels and a rigid lid at 2.914 hPa. A reference atmospheric temperature and a reference surface pressure are adopted in BCC_AGCM2.1 model, which induces substantial changes in the associated diagnostic equations and their resolving technique [*Wu et al*., 2008, 2010]. Main physical process parameterization schemes are used here as follows: the new deep penetrative convection scheme suggested by *Wu* [2012], dry adiabatic adjustment scheme [*Yan*, 1987], turbulent fluxes over ocean surface calculated by the bulk formulas [*Zeng et al*., 1998; *Collins et al*., 2006] with considering the impacts of waves and sea spray affected by the wind speed [*Wu et al*., 2010], the community land model version 3 land surface process parameterization scheme [*Oleson et al*., 2004] in which a nondimensional coefficient for snow cover fraction calculation modified by *Wu et al*. [2010], and other parameterization schemes such as radiative transfer scheme and planet boundary layer parameterization scheme which are the same as in CAM3.

3.2. Numerical Experiment Design

[18] Three experiments shown in Table 1 were carried out in this study. In the Real SST forced (RSST) experiment, an eight-member ensemble of runs with different initial conditions provided by the four times daily NCEP/NCAR reanalysis data of 1 and 2 January 2008 was performed

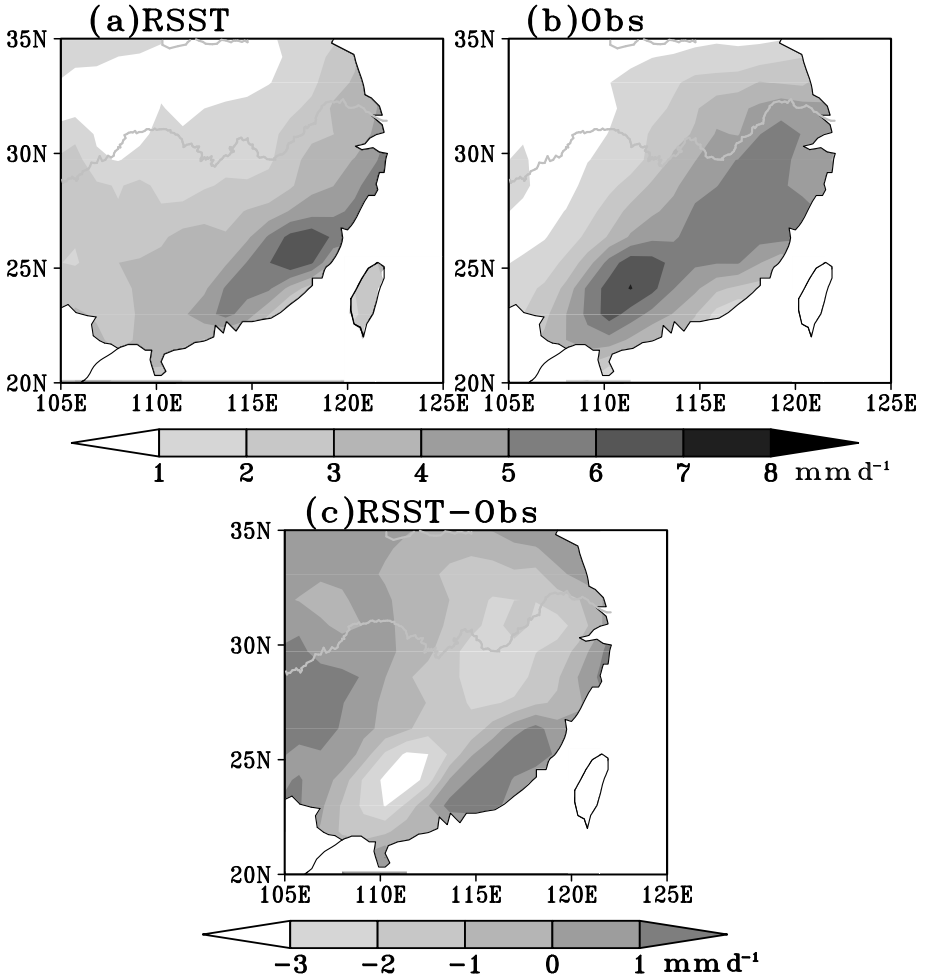

Figure 1. The (a) RSST experiment simulated and (b) observed precipitation averaged over 10 January to 2 February 2008 and (c) the differences between the simulation and observation. The grey curves show the Yangtze River and Yellow River.

during 1 January to 1 March 2008. The daily NOAA SST data and sea ice concentrations data set which was interpolated onto the model grids using bilinear interpolation method offered the boundary conditions for the BCC_AGCM2.1 model. The eight-member ensemble of runs in the SST anomaly forced (SSTA) experiment was carried out similarly to the RSST except that the BCC_AGCM2.1 was forced by the daily SST derived from the daily SST climatology in January and February for the years from 1982 to 2008 superposed by the SST anomalies on 1 January 2008. To produce a climatology data set in January and February, in the multi-year mean (MEAN) experiment runs were conducted during 1 January to 1 March in each year from 1982 to 2007. The BCC_AGCM2.1 model was initialized by the four times daily NCEP/NCAR reanalysis data of 1 January in each year of 1982–2007 and forced by the observed daily SST and sea ice concentrations data set during 1 January to 1 March in each year of 1982–2007. All the runs output daily mean results during the integrated periods in each experiment.

[19] To evaluate the 10–30 day extended range potential predictability of the BCC_AGCM2.1 model, we only focus on the analysis during the period when the heavy snow storms occurred over southern China in early 2008. First, we used the Talagrand distribution or rank histogram [*Talagrand et al.*, 1997; *Candilie and Talagrand*, 2005] which is a good index of frequencies and dispersion of the rank of observed data within the ensemble simulations to measure how well the eight ensemble simulations of the RSST experiment cover the reality. This is a necessary base of further discussion of ensemble mean. We have eight ensemble simulations which can be sorted from smallest to largest value to define nine ranks. The observation will fall into one of these ranks. It is expected that each rank should have an equal probability of covering the observation. So a good ensemble should have a uniform distribution. Talagrand distribution of the precipitation (not shown) over southern China in early 2008 displays that the probabilities have a little difference from each other and most probabilities are very close to the mean probability (11.1%) which is under the ideal situation, signifying that the ensemble system has reasonable dispersion and can well cover the reality.

[20] The comparisons of the ensemble mean of the results from the RSST runs with the observed and NCEP/NCAR reanalysis data can show us how the BCC_AGCM2.1 model's 10–30 day extended range potential predictability is. To discuss the possible physical mechanisms, we also study the anomalous atmospheric circulations on interannual time scales by analyzing the differences between the

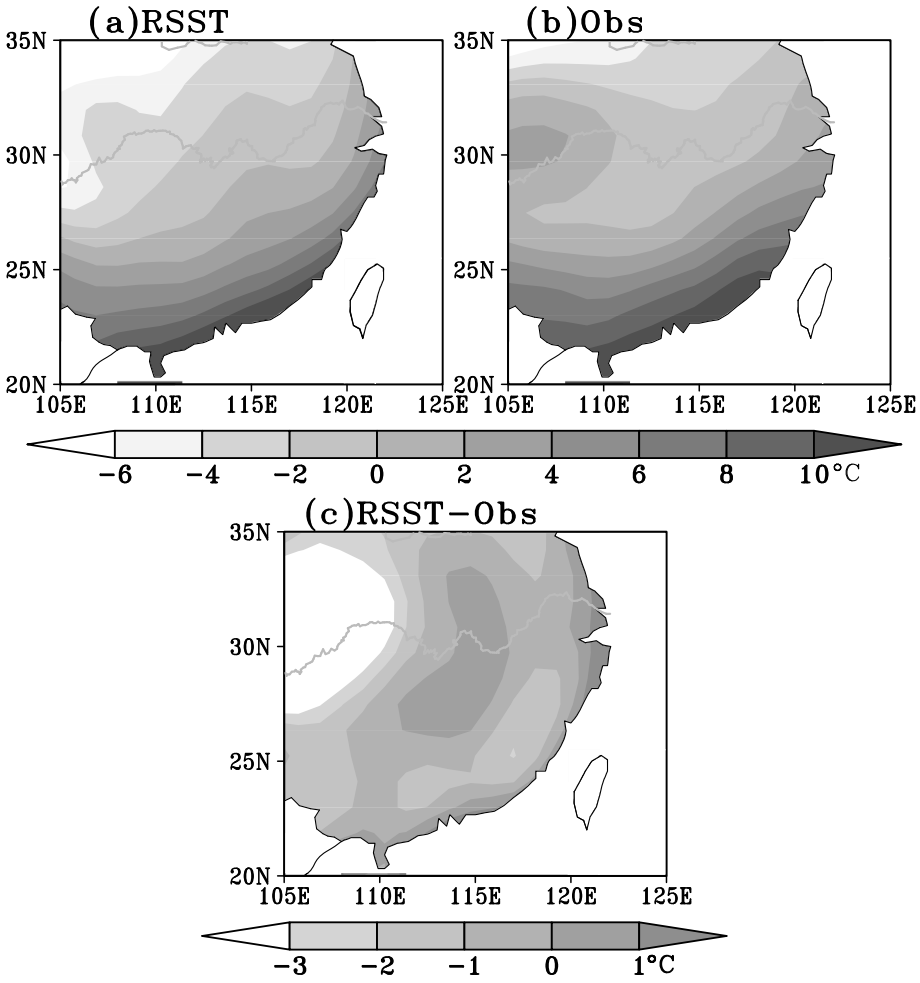

Figure 2. The (a) RSST experiment simulated and (b) observed 2 m surface air temperature averaged over 10 January to 2 February 2008 and (c) the differences between the simulation and observation. The grey curves show the Yangtze River and Yellow River.

ensemble mean of the results from the RSST runs and the 26 year (1982–2007) climatology results from the MEAN experiment during the period when the heavy snow storms happened. Comparisons of the results from the runs in SSTA experiment with those from the RSST runs are analyzed to see how the real daily SST with relatively larger day-to-day variability can affect the model's ability in simulating the heavy snow storm episodes in early 2008.

4. Results

4.1. The 10–30 Day Extended Range Potential Predictability of the BCC_AGCM2.1 Model

[21] During 10 January to 2 February 2008, southern China experienced four episodes of severe and persistent snow storm which happened during 10–16, 18–22, 25–29 January, and 31 January to 2 February 2008, respectively [*Gao*, 2009; *Wen et al*., 2009; *Zhou et al*., 2009]. For simplicity, the four episodes are called the first, second, third, and fourth snow storm event (namely SE1, SE2, SE3, and SE4) according to the time, respectively. We call the whole persistent snow storms during 10 January to 2 February 2008 SE.

[22] During the SE period, the observed precipitation (Figure 1b) displays a northeast-southwest rain belt with a maximum precipitation center over 6 mm d^{-1} located in Guangdong province. This rain belt almost covers the entire southern China. Comparisons of the simulated precipitation in Figure 1a with the observation in Figure 1b indicate that the BCC_AGCM2.1 model well reproduced the observed rain belt except for a further north maximum precipitation center located in Fujian province and underestimated precipitation on the order ranging from 1 to 3 mm d^{-1} in the main rain belt area (Figure 1c).

[23] Figure 2b gives the observed surface 2 m air temperature averaged over the SE period. It can be noted that the observed 2 m air temperature increases from the north to southeast China with a warm center over 10°C located along the southeast coastal region and a cold tongue extending to the south of the Yangtze River. Although the BCC_AGCM2.1 model produced some cold bias (Figure 2c) over most part of the southeast China, it well simulated the distribution of the observed 2 m air temperature (Figure 2b). Overall, the BCC_AGCM2.1 model has good ability in reproducing the distribution of the rainfall and 2 m air temperature during 10 January to 2 February 2008.

[24] To further provide details of the process in the snow storm period, Figure 3 gives the observed and simulated precipitation averaged over each period of the four snow storm

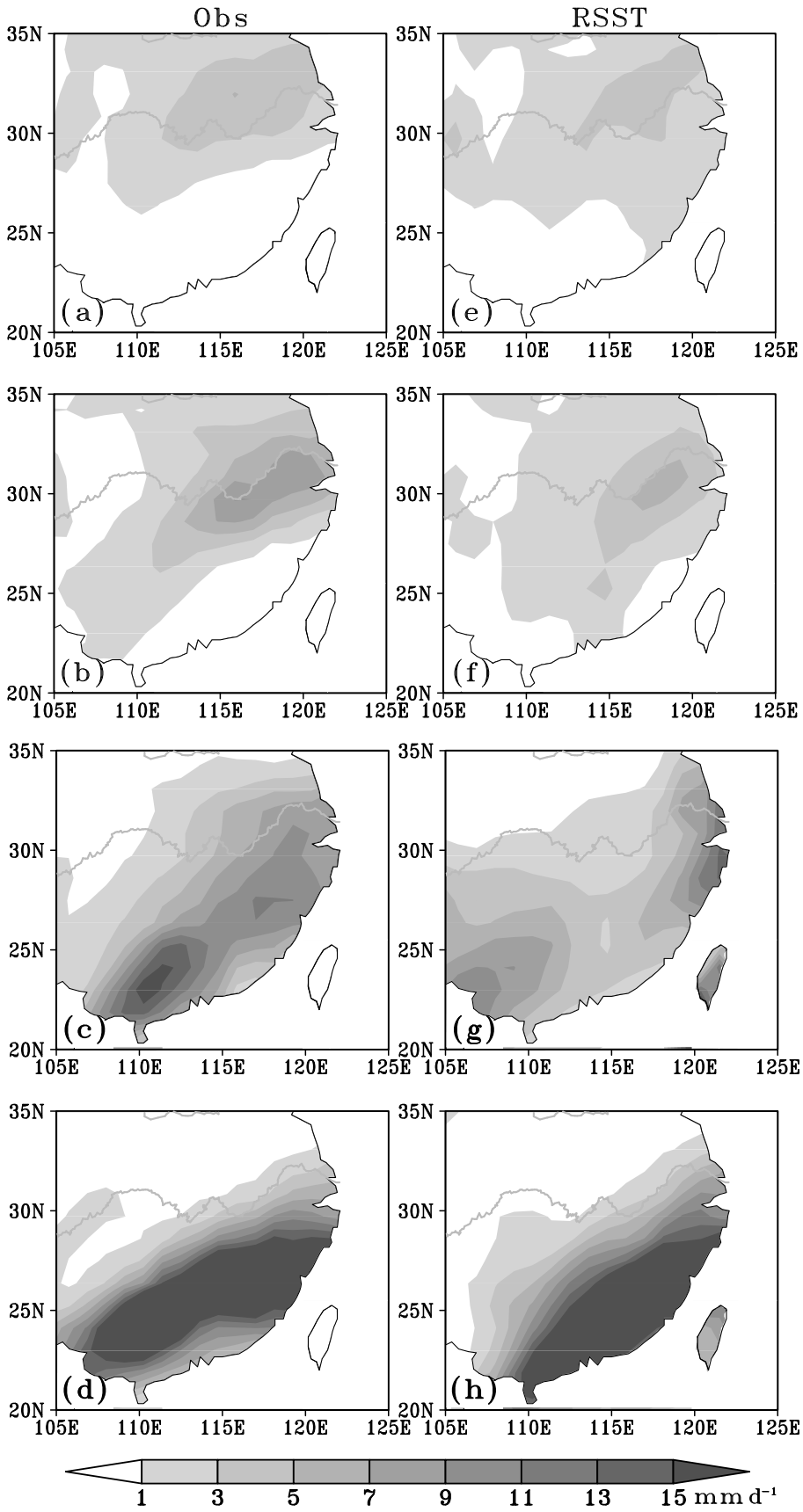

Figure 3. The (left) observed and (right) RSST experiment simulated precipitation averaged over the period of (a, e) SE1, (b, f) SE2, (c, g) SE3, and (d, h) SE4 in early 2008, respectively. The grey curves show the Yangtze River and Yellow River.

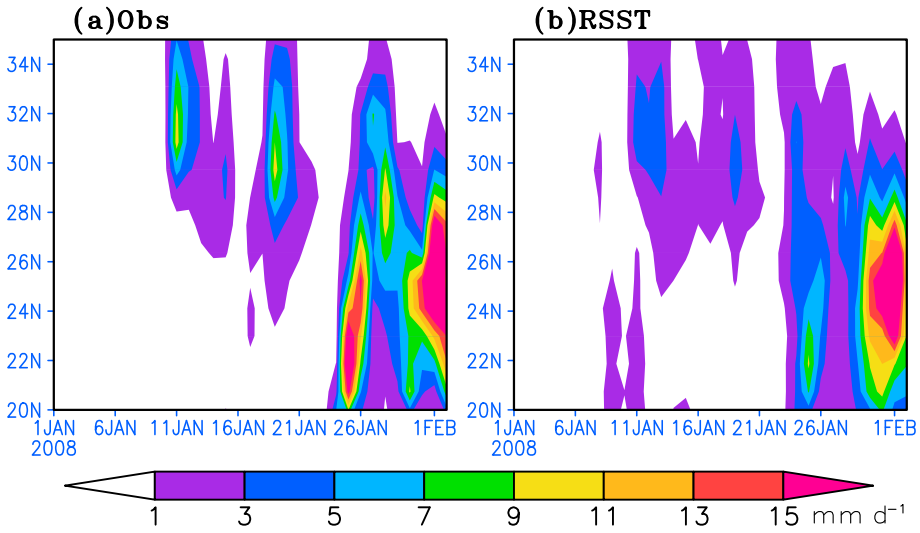

Figure 4. The time-latitude cross section of the (a) observed and the (b) RSST experiment simulated precipitation averaged along 105°E–121°E in early 2008.

events. As the observation shown in Figure 3a, during the period of the SE1, a notable west-eastward rain belt in the observation extends from Hubei province to the north region of Jiangsu province, a maximal center with the precipitation over 3 mm d^{-1} is located in the Huaihe River Basin. The observed precipitation in SE2 (Figure 3b) shows a similar distribution compared to that in the first one, except that the rainfall center with a maximum precipitation over 7 mm d^{-1} shifts southward and is located in the south of the Yangtze River. During the periods of SE3 and SE4 (Figures 3c and 3d), the precipitation intensifies and the rain belts shift to southwest-northeastward compared with those in SE1 and SE2. Especially in SE4, the precipitation is the strongest among the four snow storm events; the precipitation intensity over most part of the southern China is over 15 mm d^{-1}. From Figures 3a–3d, the observed rain belts over southeast China for the four snow storm episodes moved from north to south with the intensified precipitation. As shown in Figures 3e–3h, the BCC_AGCM2.1 model well reproduced the observed precipitation distribution for the four snow storm events except that the maximal centers of the simulated rain belts in SE4 were located in further east compared to the observation.

[25] Figure 4 displays the time-latitude cross section of the observed and simulated precipitation averaged along 105°E–121°E in early 2008. As shown in Figure 4a, it is clearly noted that the observed rain belt moves from north to south with the intensified precipitation. The BCC_AGCM2.1 model simulated this feature well except that some difference in the precipitation intensity can be noted (Figure 4b).

[26] The observed 2 m air temperature distributions during the four heavy snow storm events are shown in Figures 5a–5d. The cold air invaded from north to south over the southeast China during the period of SE1–SE3. The cold tongues with the 2 m air temperature ranging from −3 to 0°C shift from relative further north in SE1 to further south and cover much larger areas in the south of the Yangtze River in SE3. However, in SE4, the cold tongue withdraws back to a little further north and the regions with the 2 m air temperature ranging from −3 to 0°C become relatively smaller compared to that in SE3. From the RSST-simulated 2 m air temperature shown in Figures 5e−5h, it is obvious that the 2 m air temperature distributions simulated by the BCC-AGCM2.1 model are in good agreement with the observation. However, it can also be noted that the BCC_AGCM2.1 model produced a warm bias in SE4.

[27] To quantify the model errors in the precipitation and 2 m air temperature produced by the BCC_AGCM2.1 model during the period of the severe snow storms from 10 January to 2 February 2008, the RMSE and SCC between the simulation and observation in each period of the four snow storm events and the whole period of the persistent heavy snow storms in early 2008 are shown in Table 2. It can be noted that the BCC_AGCM2.1 model well reproduced the observed 2 m air temperature spatial distribution with very high SCC values larger than 0.9 which is over 99% significant confidence level. It can also be seen that the spatial distribution of precipitation simulated by the BCC_AGCM2.1 model agrees well with the observation with the SCC values above 0.6 which is over 95% significant confidence level. The RMSE of 2 m air temperature and precipitation ranges from 1.94°C to 2.40°C and 0.93 to 5.15 mm d^{-1}, respectively. It is obvious that the simulated 2 m air temperature and precipitation of SE1 which have the lowest RMSE and the highest SCC values compared to other snow storm events are the closest to the observation among the four heavy snow storm episodes.

[28] Precipitation is the result of atmospheric circulations; it is necessary to see the BCC_AGCM2.1 model's ability in simulating the atmospheric circulations. Figure 6 gives the comparisons of the RSST-simulated wind vectors at the levels from the upper to lower troposphere with the NCEP/NCAR reanalysis data. Overall, the BCC_AGCM2.1-simulated wind vectors show high consistency with the NCEP/NCAR reanalysis. The BCC_AGCM2.1 model well reproduced the westerly jet at 200 and 500 hPa levels along the zones between 20°N and 35°N. It realistically simulated the relatively strong southwest winds at 700 hPa level over the southeast China and the easterly winds at 500–850 hPa levels over low latitudes as well. The model also well simulated the clear

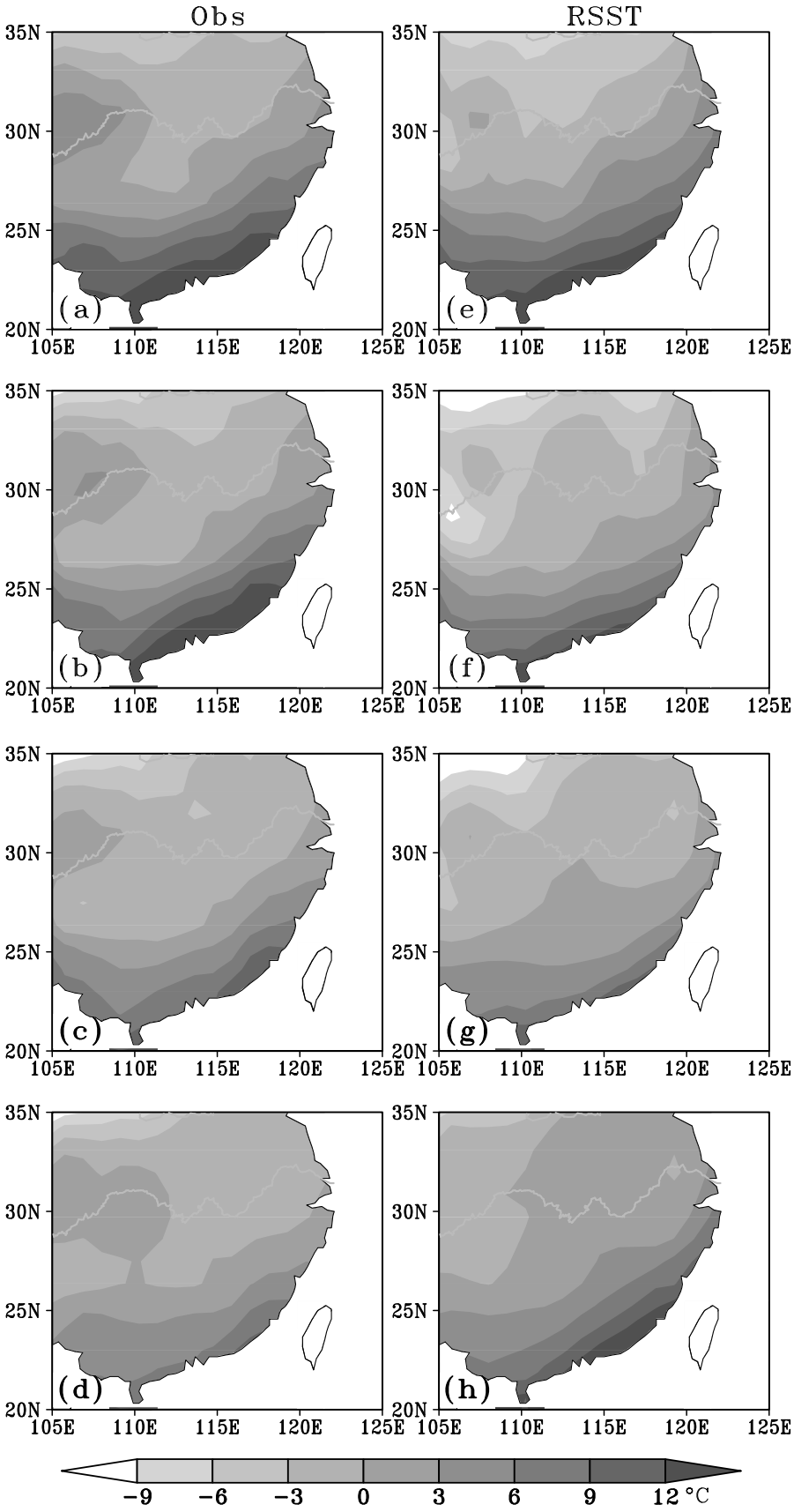

Figure 5. The (left) observed and the (right) RSST experiment simulated 2 m air temperature averaged over the period of (a, e) SE1, (b, f) SE2, (c, g) SE3, and (d, h) SE4 in early 2008, respectively. The grey curves show the Yangtze River and Yellow River.

Table 2. RMSE and SCC Between the Observed and Modeled 2 m Air Temperature and Precipitation Over Southern China in Each Period of the Four Snow Storm Events and the Whole Period of the Persistent Snow Storms During 10 January to 2 February 2008

Variables	Statistics	SE1	SE2	SE3	SE4	SE
2 m air temperature	RMSE (°C)	1.94	2.30	2.14	2.40	2.21
	SCC	0.95	0.94	0.93	0.90	0.92
Precipitation	RMSE (mm d^{-1})	0.93	1.41	3.12	5.15	1.42
	SCC	0.73	0.71	0.67	0.66	0.70

characteristic feature (Figures 6b and 6c) that the southwest air flow from the low latitudes and the northwest air flow from the high latitudes converge together over Japan and then change to westerly winds.

[29] To provide a more clearly quantitative comparison, Figure 7 gives the plots of regional mean of the daily precipitation and 2 m air temperature averaged over 20°N–35°N and 105°E–121°E from the observation and the simulation of the RSST and SSTA runs in early 2008. As shown in Figure 7a, it is clearly seen from the observation that the four snow rainfall episodes are separated from each other at a very short time interval during the snow storm period. The largest precipitation can be detected in SE4. The temporal correlation coefficient between the observed and the RSST-simulated precipitation is 0.61 which is over 95% significant confidence level, indicating that the BCC_AGCM2.1 model realistically reproduced the time series of the precipitation except for an underestimation (overestimation) of the precipitation in SE3 (SE4). However, the SSTA experiment only reproduced the precipitation of the first snow storm event. The temporal evolution of the 2 m air temperature is shown in Figure 7b. From the observation, the 2 m air temperature increased from about 7°C to 13°C before 10 January 2008 and then dramatically decreased to around 4° C in a very short time. After 14 January 2008, the cold conditions with the 2 m air temperature below 4°C lasted almost 20 days and the 2 m air temperature reached its lowest level during SE4. From the simulation of the RSST and SSTA experiments, the BCC_AGCM2.1 model well simulated the temporal variation of the observed 2 m air temperature with a temporal correlation coefficient of 0.87 despite the cold (warm) biases in SE1–SE2 (SE3–SE4).

[30] From the comparisons of the 2 m air temperature and precipitation between the RSST simulation and observation during the period of the heavy snow storms which occurred over southern China in early 2008, the BCC_AGCM2.1

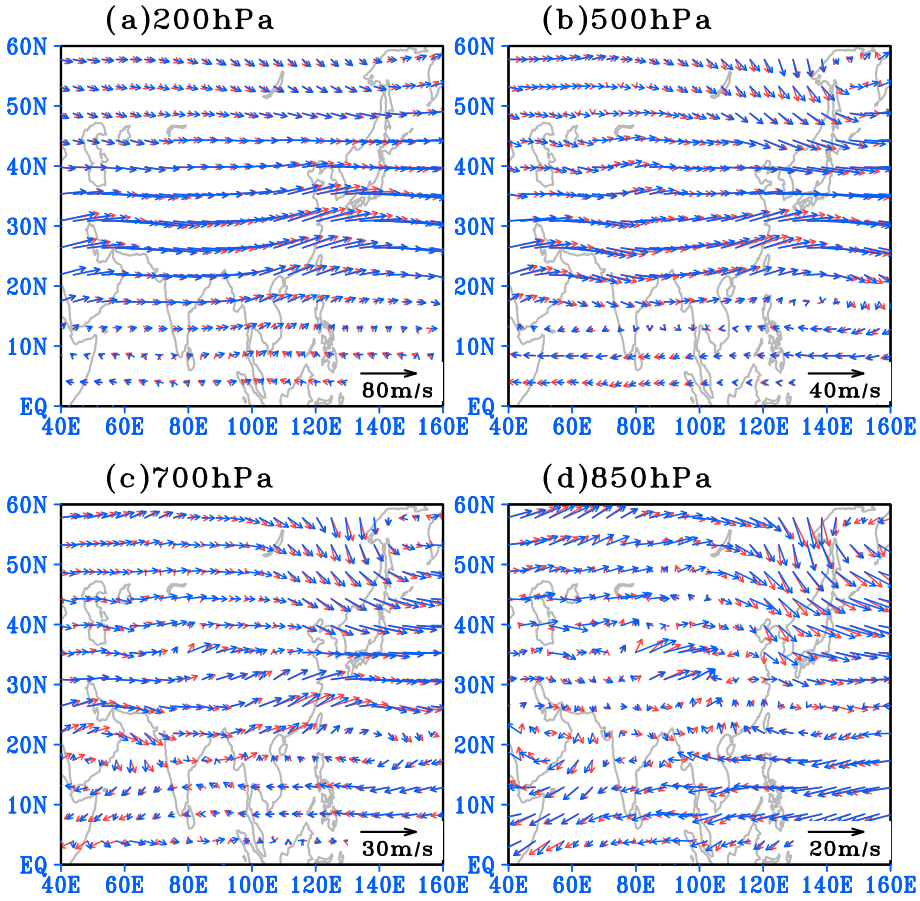

Figure 6. The NCEP/NCAR (red) and the RSST experiment simulated (blue) wind vectors averaged over 10 January to 2 February 2008 at (a) 200 hPa, (b) 500 hPa, (c) 700 hPa, and (d) 850 hPa levels.

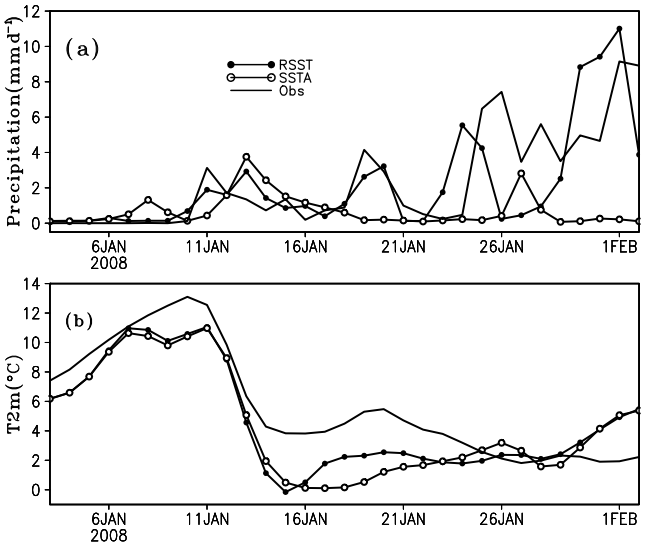

Figure 7. Time series of the observed, the RSST, and SSTA experiments simulated (a) precipitation and (b) surface 2 m air temperature regionally averaged over 20°N–35°N, 105°E–121°E in early 2008.

model well reproduced this snow storm process including the spatial distribution and temporal evolution of the 2 m air temperature and precipitation. It has good performance in simulating the weather variation at the 10–30 day extended range forecasting time scale. However, comparisons of the RSST and SSTA simulations with the observation (Figures 7a and 7b) indicate that the SSTA cannot reproduce the precipitation during SE2–SE4, despite little difference in the simulated 2 m air temperature between the RSST and SSTA experiments. From the experimental design, the RSST and SSTA runs have the same initial conditions, only the SST forcing is different. The RSST (SSTA) was forced by the real daily SST (the daily SST derived from the daily SST climatology in January and February for the years from 1982 to 2008 superposed by the SST anomalies on 1 January 2008) during 1 January to 1 March 2008. However, much difference in the simulated precipitation between the RSST and SSTA experiments can be noted. What reasons resulted in this difference? To answer this question may help us to improve our 10–30 day extended range forecasting system. Possible reasons will be discussed in the next section.

4.2. Possible Reasons

[31] To reveal the possible reasons which may significantly affect the BCC_AGCM model's ability of the 10–30 day extended range forecast, we will analyze the atmospheric variability produced by the model and the importance of SST forcing with day-to-day variability.

4.2.1. Atmospheric Circulation

[32] First, Figure 8 shows the observed and simulated anomalies of the precipitation and vertically integrated (surface to 300 hPa) water vapor transport flux averaged over the period of each snow storm event in early 2008. From the observed precipitation and vertically integrated (surface to 300 hPa) water vapor transport flux anomalies (Figures 8a–8d), it is clear that large positive precipitation anomalies appeared over Jianghuai valley (south of the Yangtze River) during the periods of SE1 and SE2 (SE3 and SE4). In particular, during the periods of SE3 and SE4, the positive precipitation anomalies occupied wider regions with much stronger intensity compared to those in SE1 and SE2. The spatial distributions of the large positive precipitation anomalies are similar to those of the large precipitation (Figures 3a–3d) during the four snow storm events. These positive precipitation anomalies are the results of the anomalous southwestward water vapor transport fluxes. It can be noted that in the RSST experiment, the BCC_AGCM2.1 model well reproduced the spatial distributions of the large positive precipitation anomalies and associated anomalous southwest water vapor transport fluxes during the four snow storm events (Figures 8e–8h), despite relatively weaker anomalies compared to the observation. However, as shown in Figures 8i–8l, in the SSTA experiment, the BCC_AGCM2.1 model only reproduced the positive precipitation anomalies and associated anomalous southwest water vapor transport fluxes during the period of SE1.

[33] *Wen et al*. [2009] found that the extraordinarily frequent and long-lasting snow storms affected southern China in January 2008 were closely linked to the intensified Middle East subtropical jet (MESJ) and the above normal subtropical western Pacific high (SWPH) which slowed down the eastward propagation of weather systems to the Pacific and favored convergence of water vapor over southern China. To see the observed and simulated large-scale climate anomalies at interannual time scales, the 200 hPa zonal wind (U200) and the 500 hPa geopotential height (HGT500) anomalies averaged over 10 January to 2 February 2008 are shown in Figures 9 and 10, respectively.

[34] As shown in Figure 9a, it is obvious from the NCEP/NCAR reanalysis that two large positive U200 anomaly centers with the intensity over 5 m s^{-1} are located over Middle East and northeast China, the Koreas and Japan, respectively. However, a weak negative U200 anomaly center can be noted over southeast China. This is consistent with the analysis of *Wen et al*. [2009] who found the MESJ was stronger than normal and the East Asian jet shifted northwestward, strengthening over northeast China and the Koreas and weakening over southern China. From Figures 9b and 9c, compared with the NCEP/NCAR U200 anomalies, the RSST well reproduced the U200 anomaly centers in the subtropical jet regions. However, the SSTA produced a negative U200 center over Middle East; this is contrary to the NCEP/NCAR data.

[35] As shown in Figure 10a, the NCEP/NCAR HGT500 anomalies were characterized by a west-low and east-high pattern over middle western Asia and tropical-subtropical China coastal area. This circulation pattern favors the intrusions of cold circulation systems from high latitudes to southern China [*Wen et al*., 2009]. The anomalous high over East Asia and the northwestern Pacific slowed down the eastward propagation of weather systems to southern China and favored convergence of water vapor, long-lasting low temperatures, and severe icing conditions over southern China. The RSST experiment (Figure 10b) well reproduced the spatial distribution pattern of the observed HGT500 anomalies. However, compared with the NCEP/NCAR reanalysis and the RSST-simulated HGT500 anomalies, the SSTA experiment (Figure10c) failed to produce the large positive HGT500 anomalies over tropical-subtropical China coastal

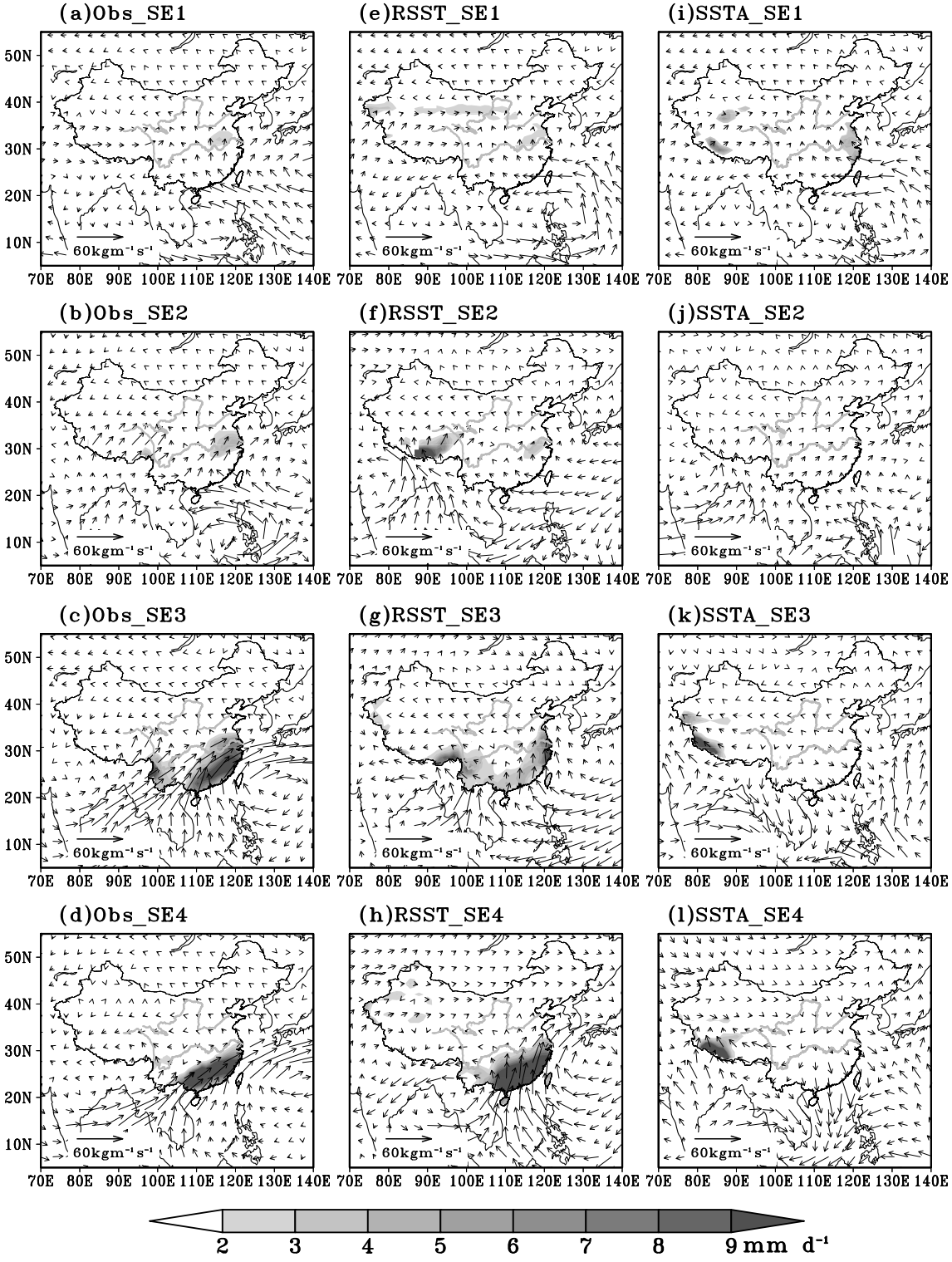

Figure 8. The (left) observed, (middle) RSST, and (right) SSTA experiments simulated anomalies of precipitation (shaded) and vertically integrated (surface to 300 hPa) water vapor transport flux (vector) averaged over the period of (a, e, i) SE1, (b, f, j) SE2, (c, g, k) SE3, and (d, h, l) SE4 in early 2008, respectively. The observed (simulated) anomalies were computed relative to the observed (MEAN simulated) climatology of 1982–2007.

area, which shifted too west and resulted in little precipitation over southern China as shown in Figure 8.

[36] To illustrate how the changes in the SST forcing affect the large-scale atmospheric circulation between the RSST and SSTA experiments, Figure 11 displays differences of 2 m air temperature and upward net heat flux at surface in Figure 11a, geopotential height, air temperature, and wind vector at 850 hPa and 200 hPa averaged over 10 January to

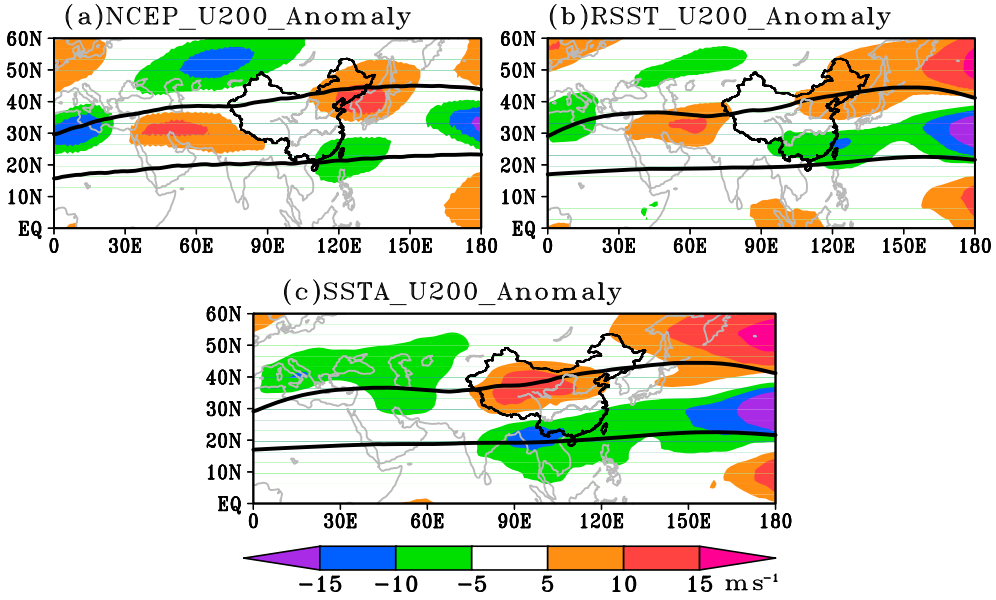

Figure 9. The anomalies of U200 averaged over 10 January to 2 February 2008. The subtropical jet regions bounded by two thick solid lines illustrate where the climatology of NCEP/NCAR (MEAN simulated) zonal winds are over 30 m s^{-1}. The NCEP/NCAR (simulated) anomalies were computed relative to the NCEP/NCAR (MEAN simulated) climatology of 1982–2007.

2 February 2008 between the RSST and SSTA experiments. As shown in Figure 11a, it can be noted that several negative (positive) 2 m air temperature difference centers are located over North Africa to Europe and north India to southern China (tropic ocean along 40°E–130°E, Middle East to central Asia and northeastern China). This distribution of the 2 m air temperature differences is consistent with the corresponding differences in the upward net heat flux at surface. The air temperature differences at 850 and 200 hPa levels (Figures 11b and 11c) show similar distribution to the 2 m air temperature differences. As expected, changes in the atmospheric thermal structure are in quadrature with the changes in surface heating (Figure 11a). This can be seen directly in the differences in the geopotential height at 200 hPa level (Figure 11c), which are the dominant contributor to the atmosphere thickness differences [*Rodwell et al*., 1999]. Two obvious positive (negative) centers of 200 hPa geopotential height differences are located over Middle East to south central Asia and northeastern China to Mongolia (Europe to northwest central Asia and north India to southwestern China). The positive (negative) meridional geopotential height gradient differences over Middle East (southern

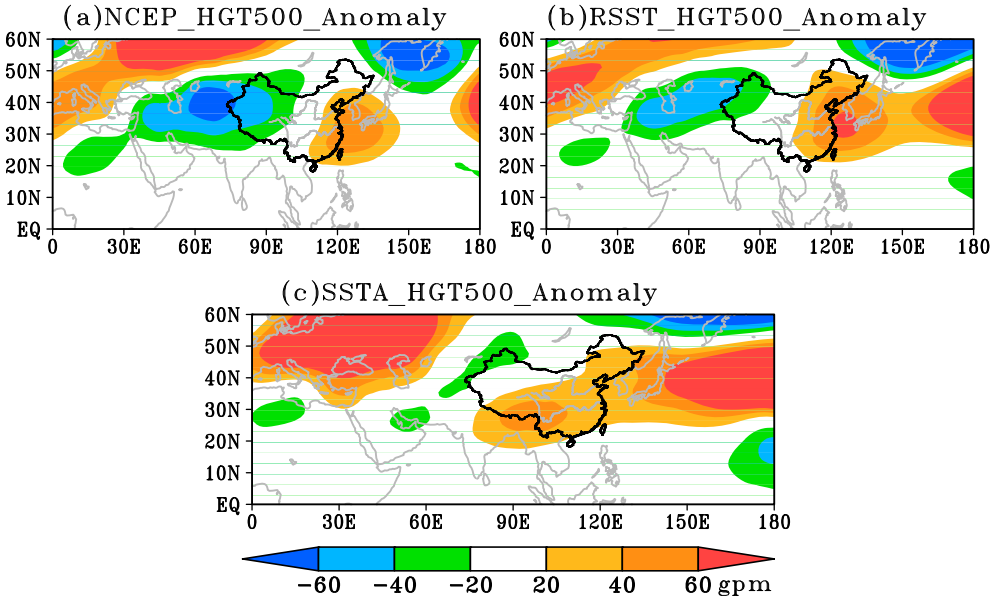

Figure 10. The anomalies of HGT500 averaged over 10 January to 2 February 2008. The NCEP/NCAR (simulated) anomalies were computed relative to the NCEP/NCAR (MEAN simulated) climatology of 1982–2007.

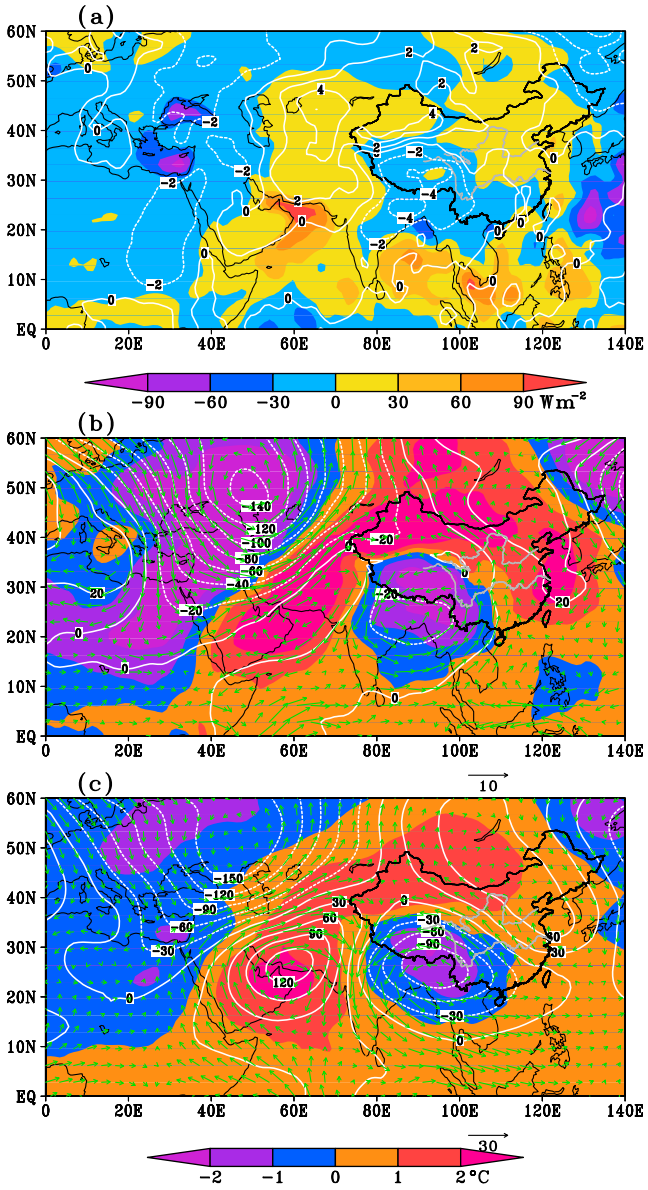

Figure 11. The differences of 2 m air temperature (contour, °C) and upward net heat flux at (a) surface (shaded, W m^{-2}), geopotential height (contour, gpm), air temperature (shaded, °C), and wind vector (m s^{-1}) at (b) 850 hPa and (c) 200 hPa between the RSST and SSTA experiments averaged over 10 January to 2 February 2008.

China) result in the strengthened (weakened) subtropical westerly jet over these regions; these differences in subtropical westerly jet agree with the results shown in Figures 9b and 9c. It also can be noted that the negative 850 hPa geopotential height difference center located over north India to southern China leads more southwesterly winds, which transport more water vapor from tropic ocean to southern China in the RSST runs than in the SSTA runs, indicating more precipitation over southern China in the RSST experiment compared to the SSTA experiment; this is consistent with the results shown in Figure 8.

[37] As mentioned above, the large-scale climate anomalies provide the background of the anomalies in the atmospheric circulations at interannual time scales which may significantly affect the extraordinarily frequent and long-lasting snow storm anomalies over southern China in early 2008. However, the synoptic scale circulation systems have direct impact on the weather variation on 10–30 day extended range forecasting time scale. It is necessary to investigate the BCC-AGCM2.1 model's ability to produce the variability in the atmospheric circulations at subseasonal time scales. Figure 12 gives the SD of the NCEP/NCAR reanalysis and simulated U200 during 1 January to 2 February 2008 which is derived from the daily data. The SD of the NCEP/NCAR U200 (Figure 12a) displays a large day-to-day variability center with the intensity over 12 m s^{-1} located over the MESJ region, where the large positive U200 anomalies can also be noted (Figure 9a). It can also be noted a relatively larger SD of NCEP/NCAR U200 over southern China, which may directly affect southern China precipitation (SCP) in early 2008; detailed analysis can be found in the following sections. In the RSST experiment (Figure 12b), the BCC_AGCM2.1 model well reproduced the observed spatial distribution of the U200 SD. However, compared with the NCEP/NCAR reanalysis and the RSST simulation, the SSTA experiment produced relatively weaker U200 SD over southern China.

[38] To reveal the atmospheric circulations associated with SCP at subseasonal time scales, Figure 13 shows the regression coefficients of the daily NCEP/NCAR reanalysis (RSST modeled) U200, HGT500, and 700 hPa wind vector on the normalized SCP of observation (RSST simulation) during 1 January to 2 February 2008 based on the linear regression method; the shaded regions indicate the correlation between each atmospheric variable and SCP over 95% significant confidence level with the absolute values of correlation coefficient above 0.35 which is the threshold for 31 (33–2) degrees of freedom at 0.05 statistical significance level. From the observation (Figures 13a–13c), the most dominant atmospheric features associated with the subseasonal variability of the SCP show significantly strengthened (decreased) U200 located over MESJ region and southern China (northwest to north China and south Mongolia), markedly declined HGT500 and strengthened southwesterlies at the lower troposphere located over southern China. These features of atmospheric patterns at the levels from upper to lower troposphere favor the SCP formation. From the RSST simulation (Figures 13d–13f), the BCC_AGCM2.1 model basically reproduced the observed atmospheric circulation patterns associated with the variability of SCP.

[39] Based on the analysis of Figures 9, 12, and 13, the U200 over MESJ region and southern China may be important to the SCP at subseasonal time scales; to further see their evolution and relation with the SCP, the time series of the NCEP/NCAR and the RSST and SSTA experiments simulated 200 hPa MESJ and southern China subtropical jet (SCSJ) regionally averaged over the area bounded by 35° E–65°E and 25°N–35°N (100°E–120°E and 20°N–35°N) are given in Figure 14a (Figure 14b). It can be noted from Figure 14a that the MESJ become gradually weaker during 1 to 15 January 2008, and then intensified with two peaks above 50 m s^{-1} on 21 and 29 January 2008, respectively. The simulated MESJ from the RSST is in good agreement with the NCEP/NCAR reanalysis data. The correlation between the NCEP/NCAR MESJ and that of the RSST is 0.72 which is over 95% significant confidence level.

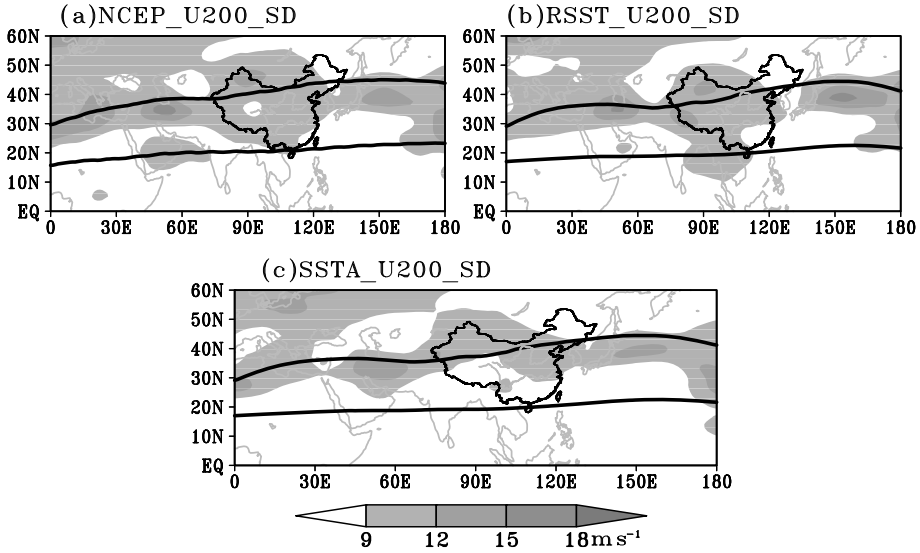

Figure 12. Distribution of the U200 SD derived from the daily U200 during 1 January to 2 February 2008. The subtropical jet regions bounded by two thick lines illustrate where the NCEP/CNAR (simulated) U200 averaged over 1 January to 2 February 2008 are over 30 m s^{-1}.

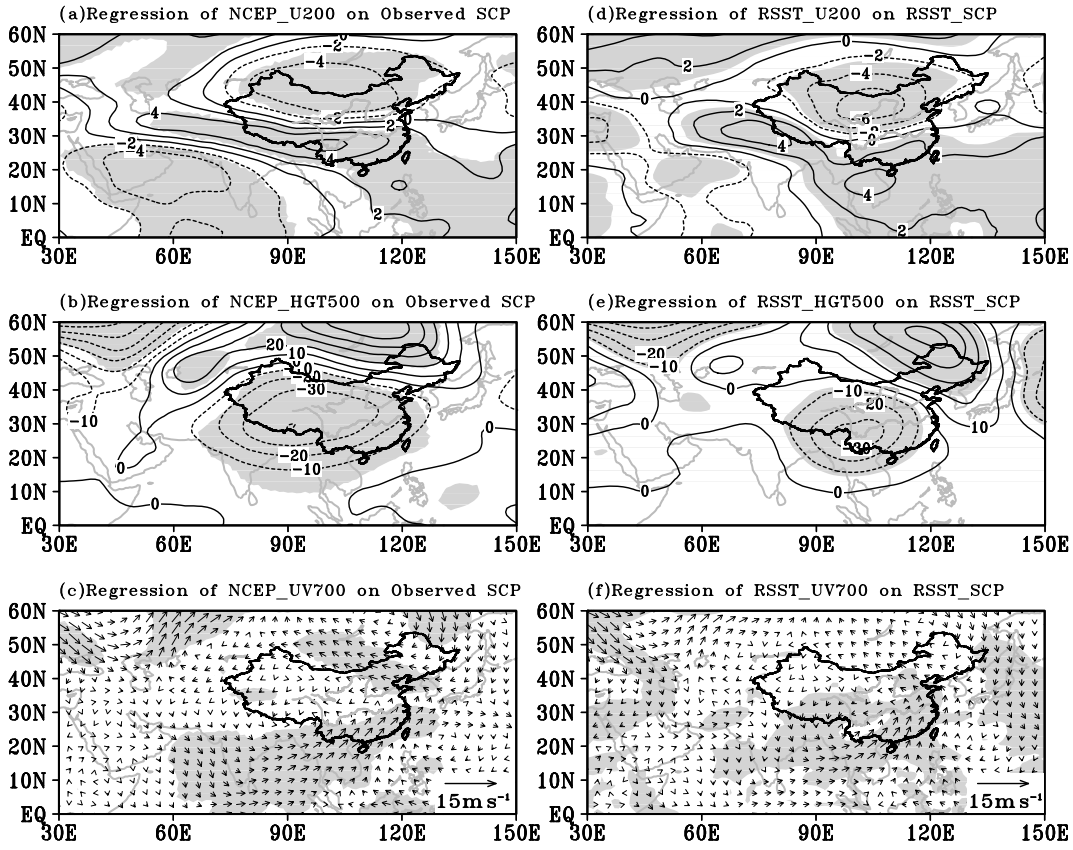

Figure 13. Regression coefficients (contour) of (a, d) the U200 (in m s^{-1}), (b, e) HGT500 (in gpm), and (c, f) 700 hPa wind vector (UV700) on the normalized SCP during 1 January to 2 February 2008. Regions over 95% significant confidence level (*t* test) are shaded. The regressions of the NCEP/NCAR reanalysis (RSST modeled) atmospheric circulations against the observed (RSST modeled) SCP are shown in left (right) panel.

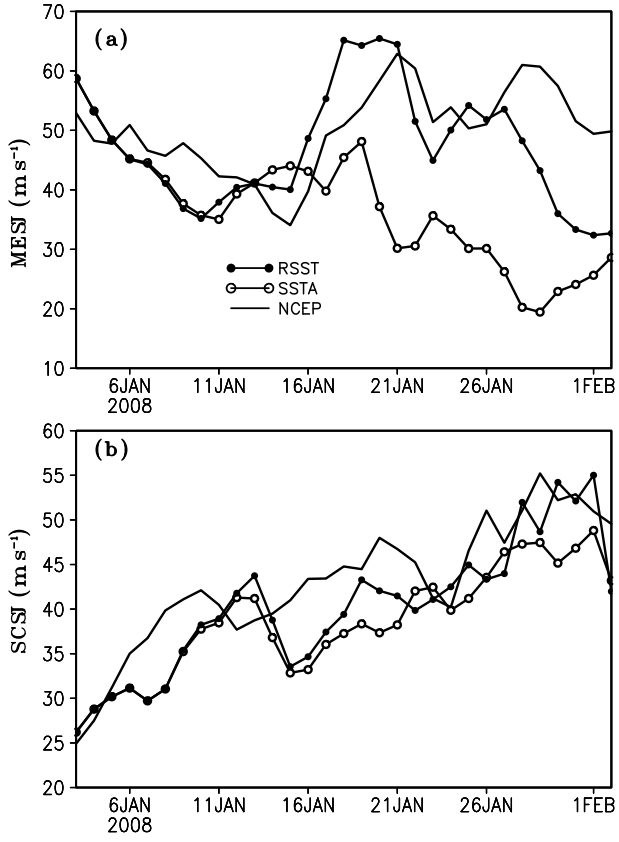

Figure 14. The time series of the NCEP/NCAR and the simulated (a) MESJ and (b) SCSJ derived from the RSST and SSTA simulated U200 regionally averaged over the area bounded by 35°E–65°E and 25°N–35°N and over the area bounded by 100°E–120°E and 20°N–35°N, respectively.

However, the SSTA experiment failed to simulate the evolution of the MESJ in NCEP/NCAR reanalysis data. As shown in Figure 14b, both RSST and SSTA experiments reproduced the strengthened SCSJ during 1 January to 2 February 2008, statistical analysis indicates that the SCSJ modeled by the RSST experiment shows higher (lower) correlation coefficient (RMSE) compared with the NCEP/NCAR reanalysis than that simulated by the SSTA experiment. Meanwhile, during 1–14 January 2008, the RSST and SSTA experiments produced almost the same MESJ (SCSJ) in Figure14a (Figure 14b), indicating that the SST forcing is not as important as the initial conditions for the weather forecast within 2 weeks in advance which is the upper limit of the daily weather forecast. However, the differences between the MESJ (SCSJ) simulated by the RSST and SSTA experiments become very large after 14 January 2008, denoting that the SST forcing plays a very important role in the 10–30 day extended range forecasts. Possible reasons related to the SST forcing will be discussed in the next section.

[40] To see how the changes in MESJ and SCSJ affect the weather variation over southern China, Figure 15a (Figure 15b) gives the lag correlation between the daily MESJ (SCSJ) and the SCP in early 2008, which is calculated based on the SCP times series during 10 January to 2 February 2008 (sample size is 24 and degrees of freedom is 22) which covers the period of long-lasting extreme snowstorms and the MESJ (SCSJ) time series derived according to the lag time, for example, the MESJ (SCSJ) time series during 2 January to 25 February 2008 is used to calculate the lag correlation coefficient when the SCP is lagged by the MESJ (SCSJ) with 8 days. From the observation, it can be noted that the strongest relation between MESJ and SCP (about 0.6, which is over 95% significant confidence level) is located at the time when the MESJ leads the SCP by 5 ~ 6 days. Earlier studies of *Wen et al*. [2009] also showed a significant positive (negative) correlation between MESJ and the precipitation (surface air temperature) over southern China in January, but on interannual time scales. Current results suggest that the early anomalous signal of the atmospheric circulations over the MESJ region may have notable influences on the severe and persistent snow storms of early 2008 at subseasonal time scales. The RSST experiment well reproduced the significant correlations when the MESJ leads the SCP by 5 ~ 6 days. However, the SSTA experiment produced weak lead correlations between the MESJ and SCP in early 2008. Meanwhile, as shown in Figure 15b, the relations between the SCSJ, which is located in the downstream of the MESJ, and the SCP in observation show a peak value (around 0.7, which is over 95% significant confidence level) at the time when the SCSJ leads the SCP by 0–1 day, indicating that the SCP is directly affected by the simultaneous SCSJ. It is clear that the RSST (SSTA) experiment well reproduced (failed to simulate) the correlation of the SCSJ with the simultaneous SCP.

[41] To further indicate how the SCSJ at upper troposphere together with the wind vector at lower troposphere vary

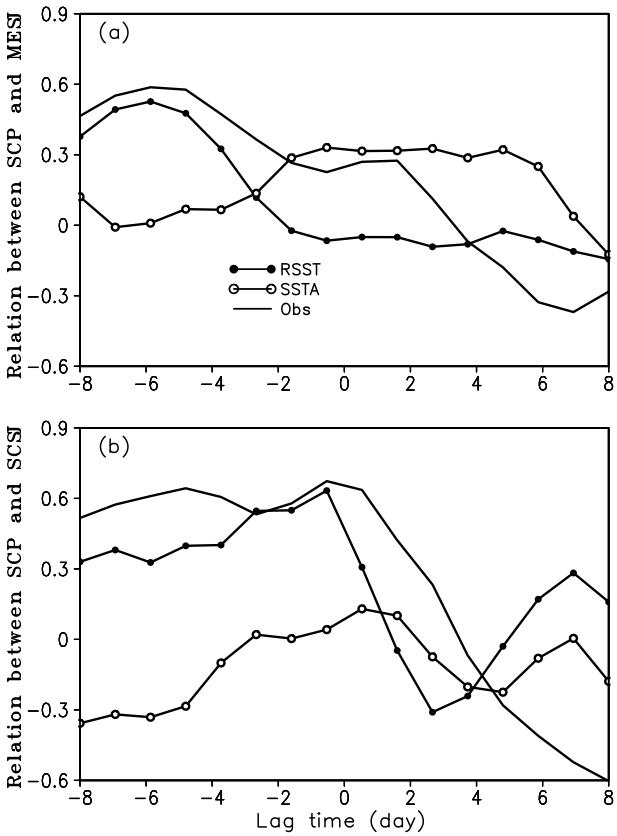

Figure 15. The lag correlations of the (a) MESJ and (b) SCSJ with the SCP in early 2008. The *x* axis shows the days of the SCP lagged by the MESJ (Figure 15a) and SCSJ (Figure 15b) during early 2008.

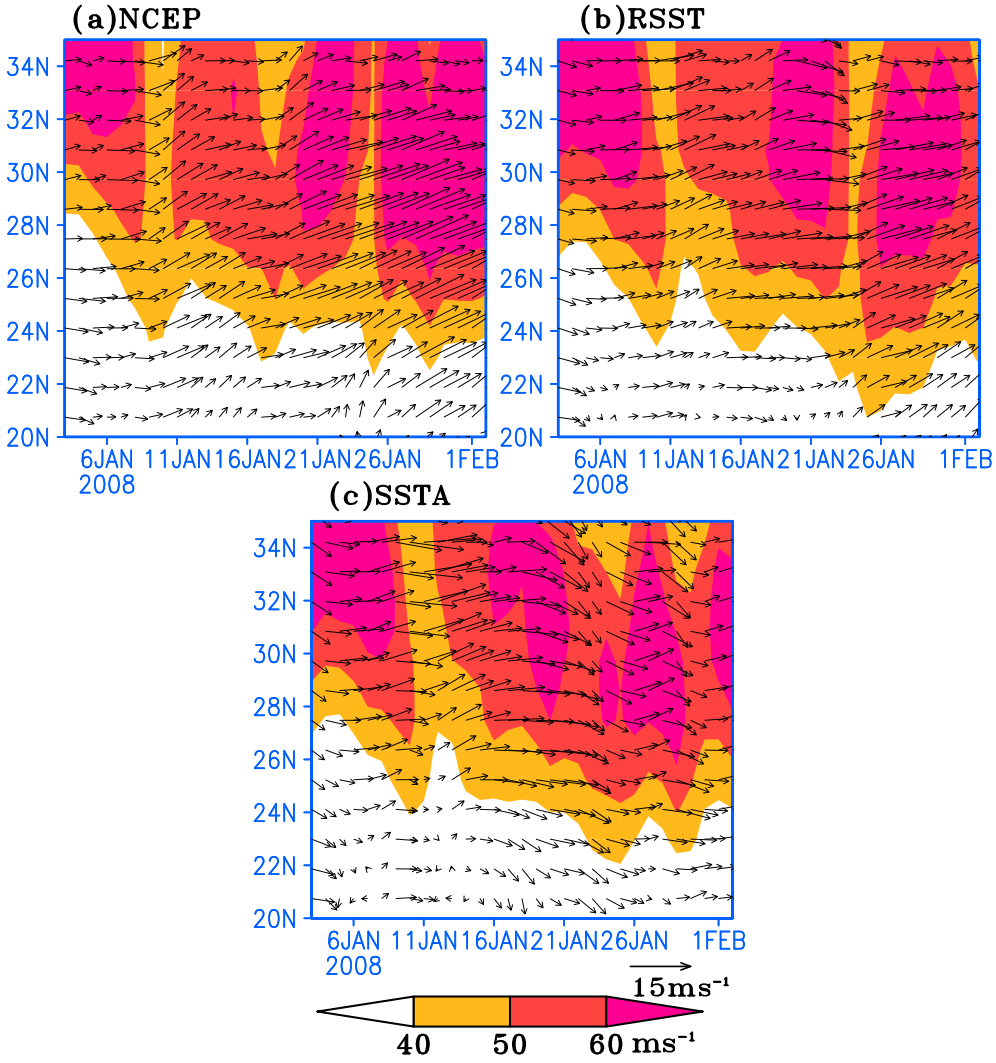

Figure 16. The time-latitude cross section of the (a) NCEP/NCAR reanalysis, (b) RSST, and (c) SSTA modeled U200 (shaded) and 700 hPa wind vectors averaged along 100°E–120°E in early 2008.

during the extremely long-lasting snow storms over southern China in early 2008, Figure 16 gives the time-latitude cross section of the NCEP/NCAR reanalysis and the BCC_AGCM2.1 modeled U200 and 700 hPa wind vector averaged along 100°E–120°E in early 2008. As shown in Figure 16a, the maximal SCSJ along the meridional region shifts from north to south with the increased intensity together with the strengthened southwest air flow at the lower troposphere located over its south side during each snowstorm event. Under the combined effects of the changes in SCSJ and southwesterly water vapor transport at lower level, the rain belt over southern China moves from north to south with the intensified precipitation in early 2008 (shown in Figure 4a). From Figure 16b, in the RSST experiment, the BCC_AGCM2.1 model well captured the spatial temporal variation of the SCSJ and lower level wind vector shown by the NCEP/NCAR reanalysis and hence the precipitation variation shown in Figure 4b. Despite that the BCC-AGCM2.1 model well simulated the SCSJ and 700 hPa wind vector before middle January 2008 in the SSTA experiment (Figure16c), it failed to reproduce them after middle January 2008, which may lead to the failure of the BCC_AGCM2.1 model in simulating the precipitation during SE2–SE4 (shown in Figure 7a).

4.2.2. Variability of the SST Forcing

[42] We have discussed the atmospheric internal variability related to the extraordinarily frequent and long-lasting snow storms over southern China in early 2008 and the differences between the simulations of the RSST and SSTA experiments in section 4.2.1. In this section, we will further reveal the reason why the simulation differences between the RSST and SSTA experiments in which the BCC_AGCM2.1 model was started from the same initial conditions but forced by different SST.

[43] First, Figure 17 gives the anomalies of SST averaged over 1 January to 2 February 2008 for the RSST and SSTA experiments. As shown in Figure 17a, the observed SST anomalies over the Pacific are dominantly characterized by the La Nina condition features, cooling (warming) appeared in the tropical central eastern Pacific (the subtropics in both hemispheres). However, the observed anomalous SST features that may not be clearly related to La Nina can also

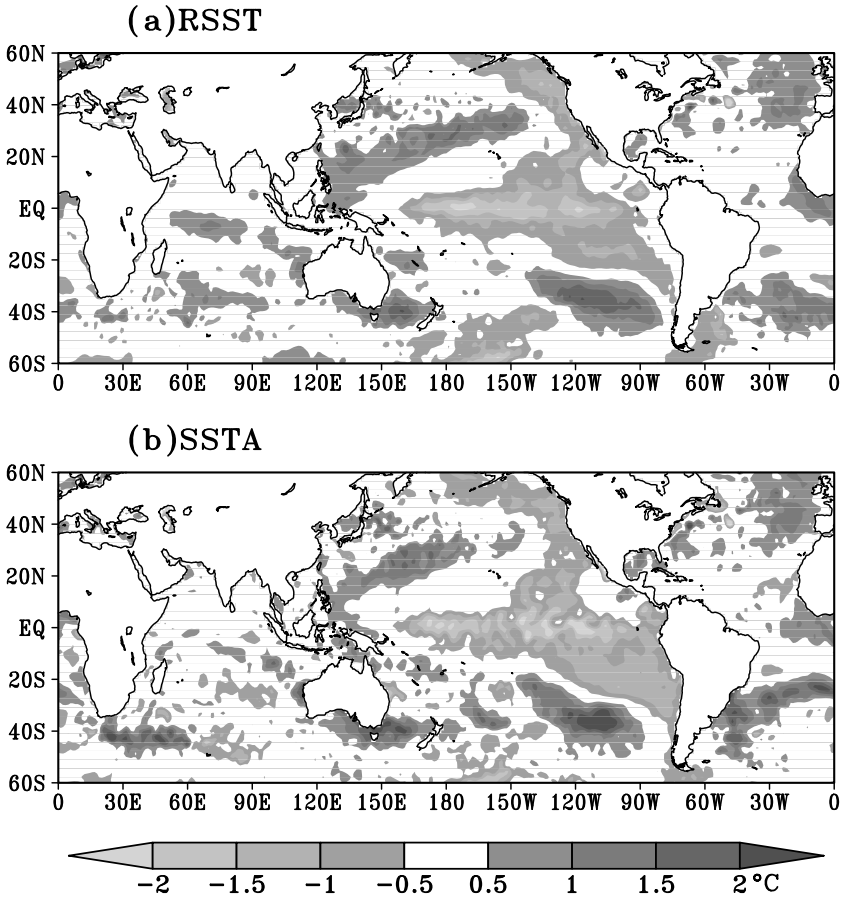

Figure 17. The SST anomalies averaged over 1 January to 2 February 2008 for the (a) RSST and (b) SSTA experiments. The anomalies were computed relative to the climatology of 1982–2008.

be noted: the warming over the subtropical northwestern Pacific and eastern North Atlantic. The daily SST forcing data for the SSTA experiment is derived from the daily SST climatology in January and February for the years from 1982 to 2008 superposed by the SST anomalies on 1 January 2008, but the anomalous SST for the SSTA experiments (shown in Figure 17b) shows very consistent spatial distribution with that in the RSST experiment.

[44] As the analysis mentioned above, the anomalous SST between the RSST and SSTA experiments show very small differences. From the experimental design, the initial conditions for the RSST and SSTA experiments are the same, only the SST forcing is different. So a question will be necessarily raised by what results in the simulation differences between the RSST and SSTA experiments. To further reveal the differences in the SST forcing, Figure 18 gives the SD of the daily SST for the RSST and SSTA experiments. As shown in Figure 18a, the SST in the RSST experiment shows a large day-to-day variability belt with the intensity around 0.5 ~ 2°C located in the subtropical ocean in the south hemisphere. Several centers with large day-to-day SST variability are located in the tropical central eastern Pacific, the subtropical northwestern Pacific, and western North Atlantic. However, the SST in the SSTA experiment (Figure 18b) shows relatively weaker day-to-day variability compared with that in the RSST experiment. We can conclude that the day-to-day SST variability mainly resulted in the differences of the simulations between the RSST and SSTA experiments at the 10–30 day extended range forecasting time scales and played an important role in the 10–30 day extended range forecast potential predictability of the BCC_AGCM2.1 model. To confirm this, an additional experiment with daily climatology SST forcing was carried out, in which the BCC_AGCM2.1 model produced very comparable precipitation and 2 m air temperature over southern China in early 2008 with the SSTA simulations (not shown), indicating that the SST variability is important to the simulation of the long-lasting snow storms in early 2008.

[45] To further indicate how the differences in SST (DSST) in the regions with the SST SD differences over 0.5°C between the RSST and SSTA experiments affect the differences of SCP (DSCP) between the RSST and SSTA experiments at the 10–30 day extended range time scales, we firstly defined a DSCP index and a DSST index, their normalized time series are shown in Figure 19. It is clear that both DSCP and DSST exhibit increasing trends with a correlation coefficient of 0.58 (over 95% significant confidence level) during 1 January to 2 February 2008, signifying that the DSST over the regions with relatively larger SST day-to-day variability significantly affect the modeled DSCP between the RSST and SSTA experiments at subseasonal time scales.

[46] To see the detailed features of the differences in the atmospheric circulations related to the DSST and DSCP at

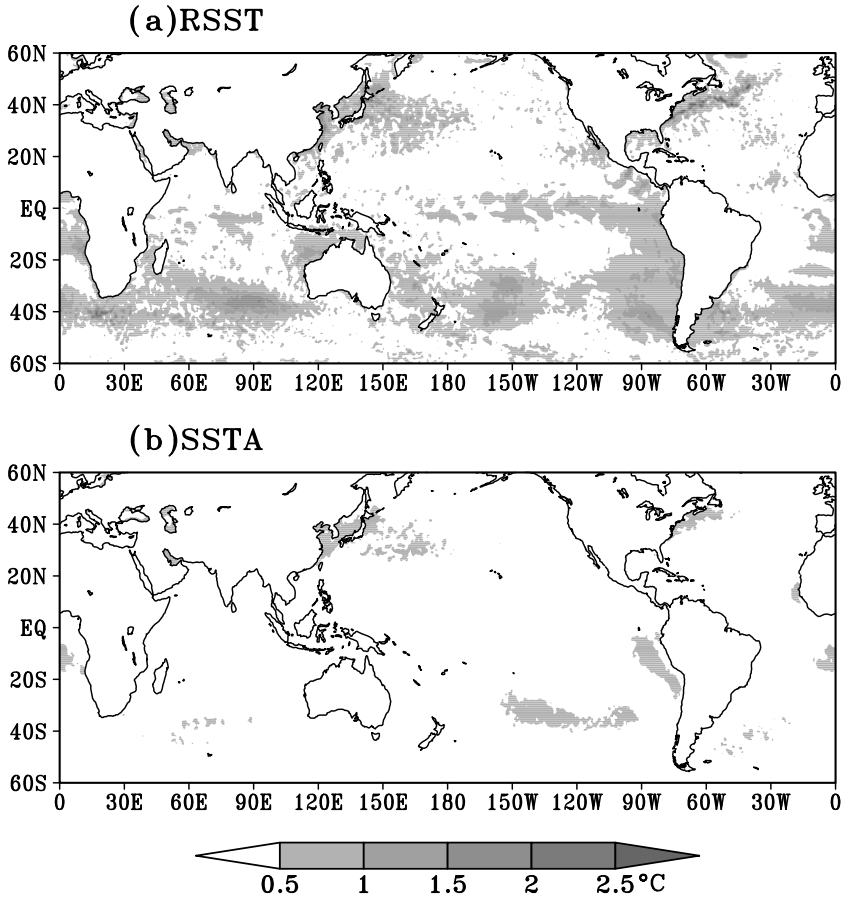

Figure 18. The SST SD derived from the daily SST forcing data for the (a) RSST and (b) SSTA experiments during 1 January to 2 February 2008.

subseasonal time scales, Figure 20 gives the regressions (similar to those shown in Figure 13) of the daily differences in the atmospheric circulations between the RSST and SSTA experiments at the levels from upper to lower troposphere on the DSST and DSCP (shown in Figure 19) in early 2008. As shown in Figures 20a–20c, it is clearly noted that compared with the SSTA runs, the RSST experiment produced significantly strengthened (weakened) 200 hPa westerlies located over the MESJ and SCSJ regions (northwest to north China and south Mongolia) during the period of the extreme snow storms in early 2008. Meanwhile, the RSST experiment simulated significantly declined 500 hPa geopotential height and strengthened southwesterlies at the lower troposphere located over southern China compared with those produced by the SSTA experiment in each snow storm events. These features of the differences in the atmospheric circulations associated with DSST from upper to lower troposphere between the RSST and SSTA experiments show similar features shown in Figure 13. From Figures 20d–20f, the regressions of the differences in atmospheric circulations on the DSCP display large resemblance to the features shown in Figures 20a–20c. The analysis of Figures 19 and 20 further confirms that the SST day-to-day variability plays a very important role in the performance of the BCC_AGCM2.1 model in simulating the SCP on the 10–30 day extended range forecasting time scale through affecting the atmospheric variability.

5. Conclusion and Discussion

[47] In this paper, we evaluated the 10–30 day extended range potential predictability of the BCC_AGCM2.1 model forced by the real daily SST and revealed some possible factors which may play important roles in the 10–30 day extended range forecasting performance of the climate model through a case study of the long-lasting extreme snow storms

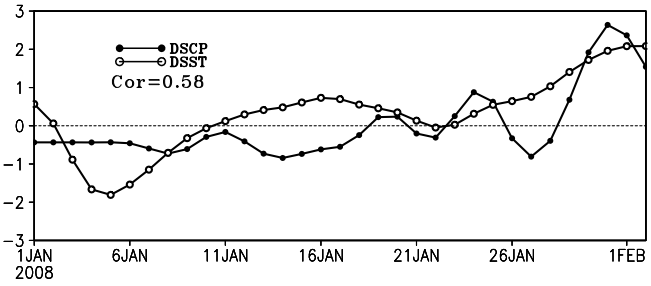

Figure 19. The normalized time series of the differences of SCP (DSCP) regionally averaged over the region bounded by 20°N–35°N and 105°E–121°E and the differences in SST (DSST) regionally averaged over the regions where the SST SD differences between the RSST and SSTA experiments are larger than 0.5°C. The differences are calculated between RSST and SSTA.

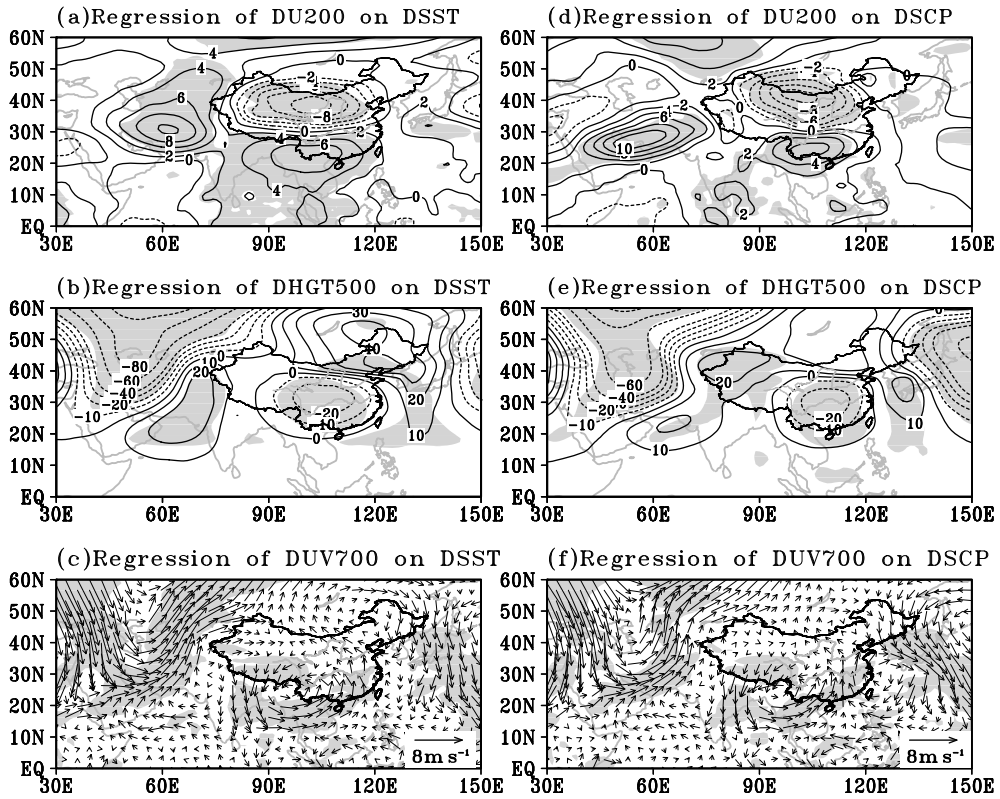

Figure 20. Regression coefficients (contour) of the differences in (a, d) U200 (DU200, in m s^{-1}), (b, e) HGT500 (DHGT500, in gpm), and (c, f) 700 hPa wind vector (DUV700, in m s^{-1}) against the normalized (left) DSST and (right) DSCP during 1 January to 2 February 2008. The differences are calculated between RSST and SSTA. Regions over 95% significant confidence level (*t* test) are shaded.

over southern China in early 2008. From the comparisons of the 2 m air temperature, precipitation, and the associated large-scale atmospheric circulations at different vertical levels between the simulation results of the RSST in which the BCC_AGCM2.1 model is forced by the observed daily SST and the observation data during the period of the extraordinarily frequent and long-lasting heavy snow storms over southern China in early 2008, the BCC_AGCM2.1 model forced by the real daily SST well reproduced this extreme snow storm process including the spatial distribution and temporal evolution of the 2 m air temperature and precipitation. It shows good performance in simulating the weather variation on the 10–30 day extended range forecasting time scale at least for this event.

[48] To further reveal the possible reasons which may significantly affect the BCC_AGCM2.1 model's ability in simulating the weather variation on the 10–30 day extended range forecasting time scale, we analyzed the differences in the simulation between the RSST and SSTA experiments in which the BCC_AGCM2.1 model forced by different SST with the same initial conditions and discussed the importance of the atmospheric variability produced by the model and SST forcing with relatively larger day-to-day variability for the climate model performance on 10–30 day extended range forecasting time scale. Compared with the RSST experiment, the SSTA experiment only produced similar precipitation of the first snow storm event in early 2008. However, both RSST and SSTA experiments simulated very similar temporal variation of the regional mean 2 m air temperature over southern China during the period of the whole snow storm in early 2008. From the climate anomalies of large atmospheric circulations at interannual time scales including water vapor transport fluxes, U200 and HGT500 which provide the background of the large-scale anomalies significantly affecting the extraordinarily frequent and long-lasting snow storms over southern China in early 2008, the RSST experiment well reproduced the positive precipitation anomalies and associated anomalous water vapor transport fluxes during the four snow storm events, the intensified 200 hPa MESJ and SCSJ, and the above normal 500 hPa SWPH in early 2008. However, the SSTA experiment only reproduced the positive precipitation anomalies and associated anomalous water vapor transport fluxes during the period of SE1 and failed to simulate the anomalies of 200 hPa MESJ and SCSJ and 500 hPa SWPH during the whole snow storm process. These anomalous features can be explained by the differences in the simulated atmospheric thermal structure and hence the meridional geopotential height gradient between the RSST and SSTA experiments. From the experimental design, the initial conditions for the RSST and SSTA experiments are the same, only the SST forcing is different. Although the differences in the anomalous SST forcing between the RSST and SSTA experiments are very small, the differences of the day-to-day SST variability between the RSST and SSTA experiments are much larger. From the analysis at subseasonal time scales, the differences of the simulated time series of the 2 m air temperature, precipitation, MESJ, and SCSJ between the RSST and SSTA

experiments are very small within 2 weeks integration, indicating that the SST forcing is not as important as the initial conditions for the weather forecast within 2 weeks in advance which is the upper limit of the daily weather forecast. However, the differences in the simulation between the RSST and SSTA experiments become much larger for the forecasting time longer than 2 weeks in advance. Further analysis of the relation of the DSST over the regions with relatively larger SST day-to-day variability with the simulated DSCP between the RSST and SSTA experiments and the atmospheric circulation differences related to the DSST at subseasonal time scales confirms that the day-to-day SST variability plays a key role in the performance of the BCC_AGCM2.1 model on the 10–30 day extended range forecasting time scale through affecting the atmospheric internal variability.

[49] We primarily revealed the potential predictability of the BCC_AGCM2.1 model on the 10–30 day extended range forecasting time scale and discussed how the SST forcing affected the BCC_AGCM2.1 model's performance of the 10–30 day extended range simulation from a case study. The results obtained in this study may provide some necessary and valuable information for the further development of the 10–30 day extended range operational forecasting system. It needs to be pointed out that in current study, the BCC_AGCM2.1 model forced by the real daily SST shows good 10–30 day extended range forecasting performance. However, we do not have the real SST data when we use BCC_AGCM2.1 model to conduct operational 10–30 day extended range forecasts. Although we tried a 10–30 day extended range forecast in the SSTA experiment to some extent, comparisons of the results from the SSTA and RSST experiments showed that the SST forcing played an important role in the 10–30 day extended range forecast. To complete an operational 10–30 day extended range forecasting system, we need to set up a dynamic or a statistical global SST prediction system to provide the BCC_AGCM2.1 model global SST data with high accuracy in the future work. In addition, we found that the subseasonal SST variability plays an important role in the SCP subseasonal variation; however, what are the specific processes through which the subseasonal SST variability affects the SCP subseasonal variation on 10–30 day extended range forecasting time scale is still an open question; further statistical and numerical studies are needed to address this question in the future work.

[50] **Acknowledgments.** We are grateful to NCEP/NCAR for allowing us to use the reanalysis data. We thank NOAA for providing the daily SST data. We also thank Steve Ghan and three anonymous reviewers for providing constructive comments that helped improve the original manuscript. We acknowledge the support by the National Science and Technology Support Project (grant 2009BAC51B03), the Special Program for China Meteorology Trade (grant GYHY201306020), the National Natural Science Foundation of China (grants 41175086 and 41105069), "the Priority Academic Program Development of Jiangsu Higher Education Institutions," and "the Fundamental Research Funds for the Central Universities" (grant 1116020701).

References

Baldwin, M. P., D. W. J. Thompson, E. F. Shuckburgh, W. A. Norton, and N. P. Gillet (2003), Weather from the stratosphere, *Science*, *301*, 317–319, doi:10.1126/science.1085688.

Baumhefner, D. P. (1996), Numerical extended-range prediction: Forecast skill using a low-resolution climate model, *Mon. Weather Rev.*, *124*, 1965–1980.

Candilie, G., and O. Talagrand (2005), Evaluation of probabilistic prediction system for a scalar variable, *Q. J. R. Meteorol. Soc.*, *131*, 2131–2150.

Cane, M. A., S. E. Zebiak, and S. C. Dolan (1986), Experimental forecasts of El Nino, *Nature*, *321*, 827–832.

Chen, T. C., and J. C. Alpert (1990), Systematic errors in the annual and intraseasonal variations of the planetary-scale divergent circulation in NMC medium-range forecasts, *Mon. Weather Rev.*, *118*, 2607–2623.

Chou, J., Z. Zheng, and S. Sun (2010), The think about 10-30 d extended range numerical weather prediction strategy facing the atmosphere chaos, *Sci. Meteorol. Sin. (in Chinese)*, *30*(5), 569–573.

Collins, W. D., et al. (2006), The formulation and atmospheric simulation of the Community Atmosphere Model version 3 (CAM3), *J. Clim.*, *19*, 2,144–2,161, doi:10.1175/JCLI3760.1.

Dickinson, R. E. (1968), Planetary waves propagating vertically through weak westerly wind wave guides, *J. Atmos. Sci.*, *25*, 984–1,002.

Ferranti, L., T. N. Palmer, F. Molteni, and K. Klinker (1990), Tropical–extratropical interaction associated with the 30–60 day oscillation and its impact on medium and extended range prediction, *J. Atmos. Sci.*, *47*, 2177–2199.

Gao, H. (2009), China's snow disaster in 2008, who is the principal player, *Int. J. Climatol.*, *29*, 2,191–2,196, doi:10.1002/joc.1859.

Huang, A., Y. Zhang, and J. Zhu (2009), Effects of the physical ensemble technique on simulation of the summer precipitation over China, *Acta Meteorol. Sin.*, *6*, 713–724.

Jin, R., J. Ma, and B. Bi (2010), Research advancement and operation status about the extended range forecast from 10 to 30 days, *Desert and Oasis Meteorol. (in Chinese)*, *2*, 1–5.

Kalnay, E., et al. (1996), The NCEP/NCAR 40-year reanalysis project, *Bull. Am. Meteorol. Soc.*, *77*, 437–471.

Kenney, J. F., and E. S. Keeping (1962), Linear regression and correlation, in *Mathematics of Statistics*, Pt. 1, 3rd ed., Chap.15, pp. 252–285, Van Nostrand, Princeton, N. J.

Li, J., and J. X. L. Wang (2003), A modified zonal index and its physical sense, *Geophys. Res. Lett.*, *30*(12), 1632, doi:10.1029/2003GL017441.

Lorenz, E. N. (1963), Deterministic nonperiodic flow, *J. Atmos. Sci.*, *20*, 130–141.

Ma, N., Y. Li, and J. Ju (2011), Intraseasonal oscillation characteristics of extreme cold, snowy and freezing rainy weather in southern China in early 2008, *Plateau Meteorol. (in Chinese)*, *30*(2), 318–327.

Matsuno, T. (1970), Vertical propagation of stationary planetary waves in the winter Northern Hemisphere, *J. Atmos. Sci.*, *27*, 871–883.

Miyakoda, K., T. Gordon, and R. Carerly (1983), Simulation of a blocking event in January 1977, *Mon. Weather Rev.*, *111*, 846–869.

Miyakoda, K., J. Sirutis, and J. Ploshay (1986), One-month forecast experiments—Without anomaly boundary forcings, *Mon. Weather Rev.*, *114*(12), 2363–2401.

Oleson, K. W., et al. (2004), Technical description of the community land model (CLM), *Technical report NCAR/TN-461STR*, National Center for Atmospheric Research, Boulder, Colorado, 174 pp.

Palmer, T. N. (1993), Extended-range atmospheric prediction and the Lorenz model, *Bull. Am. Meteorol. Soc.*, *74*, 49–65.

Reynolds, R. W., T. M. Smith, C. Liu, D. B. Chelton, K. S. Casey, and M. G. Schlax (2007), Daily high-resolution-blended analyses for sea surface temperature, *J. Clim.*, *20*, 5,473–5,496, doi:10.1175/2007JCL1824.1.

Rodwell, M. J., D. P. Rowell, and C. K. Folland (1999), Oceanic forcing of the wintertime North Atlantic Oscillation and European climate, *Nature*, *398*, 320–333.

Scaife, A. A., and J. R. Knigh (2008), Ensemble simulations of the cold European winter of 2005–2006, *Q. J. R. Meteorol. Soc.*, *134*, 1647–1659.

Shukla, J. (1981), Dynamical predictability of monthly means, *J. Atmos. Sci.*, *38*, 2547–2572.

Simmons, A. J., and A. Hollingsworth (2002), Some aspects of the improvement in skill of numerical weather prediction, *Q. J. R. Meteorol. Soc.*, *128*, 647–677.

Smith, D. M., A. A. Scaife, and B. Kirtman (2012), What is the current state of scientific knowledge with regard to seasonal and decadal forecasting? *Environ. Res. Lett.*, *7*, 015602, doi:10.1088/1748-9326/7/1/015602.

Talagrand, O., R. Vautard, and B. Strauss (1997), Evaluation of probabilistic prediction systems, *Proc. ECMWF Workshop on Predictability*, Reading, United Kingdom, ECMWF, 1–26.

Van Den Dool, H. M., and S. Saha (1990), Frequency dependence in forecast skill, *Mon. Weather Rev.*, *118*, 128–137.

Waliser, D. E., C. Jones, J. E. Schemm, and N. E. Graham (1999), A statistical extended-range tropical forecast model based on the slow evolution of the Madden–Julian oscillation, *J. Clim.*, *12*, 1918–1939.

Wen, M., Y. Song, A. Kumar, and P. Zhang (2009), An analysis of the large-scale climate anomalies associated with the snowstorms affecting China in

January 2008, *Mon. Weather Rev.*, *137*, 1,111–1,131, doi:10.1175/2008MWR2638.1.

Wu, T. (2012), A mass-flux cumulus parameterization scheme for large-scale models: Description and test with observations, *Clim. Dyn.*, *38*, 725–744, doi:10.1007/s00382-011-0995-3.

Wu, T., R. Yu, and F. Zhang (2008), A modified dynamic framework for atmospheric spectral model and its application, *J. Atmos. Sci.*, *65*, 2,235–2,253, doi:10.1175/2007JAS2514.1.

Wu, T., R. Yu, F. Zhang, Z. Wang, M. Dong, L. Wang, X. Jin, D. Chen, and L. Li (2010), The Beijing Climate Center atmospheric general circulation model: Description and its performance for the present-day climate, *Clim. Dyn.*, *34*, 149–150, doi:10.1007/s00382-008-0487-2.

Wu, T., et al. (2013), Global carbon budgets simulated by the Beijing Climate Center Climate System Model for the last century, *J. Geophys. Res. Atmos.*, *118*, 4,326–4,347, doi:10.1002/jgrd.50320.

Yan, H. (1987), Design of a nested fine-mesh model over the complex topography. Part two: Parameterization of the subgrid physical processes, *Plateau Meteorol. (in Chinese)*, *6*(suppl), 64–139.

Zeng, X., M. Zhao, and R. E. Dickinson (1998), Intercomparison of bulk aerodynamic algorithms for the computation of sea surface fluxes using TOGA COARE and TAO data, *J. Clim.*, *11*, 2628–2644.

Zhou, W., J. C. L. Chan, W. Chen, J. Ling, J. G. Pinto, and Y. Shao (2009), Synoptic-scale controls of persistent low temperature and icy weather over southern China in January 2008, *Mon. Weather Rev.*, *137*, 3978–3991, doi:10.1175/2009MWR2952.1.